



This is a repository copy of *Biomedical applications of the dynamic nuclear polarization and parahydrogen induced polarization techniques for hyperpolarized 13C MR imaging*.

White Rose Research Online URL for this paper:
<https://eprints.whiterose.ac.uk/160143/>

Version: Published Version

Article:

Stewart, N.J. orcid.org/0000-0001-8358-394X and Matsumoto, S. (2021) Biomedical applications of the dynamic nuclear polarization and parahydrogen induced polarization techniques for hyperpolarized 13C MR imaging. *Magnetic Resonance in Medical Sciences*, 20 (1). pp. 1-17. ISSN 1347-3182

<https://doi.org/10.2463/mrms.rev.2019-0094>

Reuse

This article is distributed under the terms of the Creative Commons Attribution-NonCommercial-NoDerivs (CC BY-NC-ND) licence. This licence only allows you to download this work and share it with others as long as you credit the authors, but you can't change the article in any way or use it commercially. More information and the full terms of the licence here: <https://creativecommons.org/licenses/>

Takedown

If you consider content in White Rose Research Online to be in breach of UK law, please notify us by emailing eprints@whiterose.ac.uk including the URL of the record and the reason for the withdrawal request.



eprints@whiterose.ac.uk
<https://eprints.whiterose.ac.uk/>

REVIEW

Biomedical Applications of the Dynamic Nuclear Polarization and Parahydrogen Induced Polarization Techniques for Hyperpolarized ^{13}C MR Imaging

Neil J. Stewart and Shingo Matsumoto*

Since the first pioneering report of hyperpolarized $[1-^{13}\text{C}]$ pyruvate magnetic resonance imaging (MRI) of the Warburg effect in prostate cancer patients, clinical dissemination of the technique has been rapid; close to 10 sites worldwide now possess a polarizer fit for the clinic, and more than 30 clinical trials, predominantly for oncological applications, are already registered on the US and European clinical trials databases. Hyperpolarized ^{13}C probes to study pathophysiological processes beyond the Warburg effect, including tri-carboxylic acid cycle metabolism, intra-cellular pH and cellular necrosis have also been demonstrated in the preclinical arena and are pending clinical translation, and the simultaneous injection of multiple co-polarized agents is opening the door to high-sensitivity, multi-functional molecular MRI with a single dose. Here, we review the biomedical applications to date of the two polarization methods that have been used for *in vivo* hyperpolarized ^{13}C molecular MRI; namely, dissolution dynamic nuclear polarization and parahydrogen-induced polarization. The basic concept of hyperpolarization and the fundamental theory underpinning these two key ^{13}C hyperpolarization methods, along with recent technological advances that have facilitated biomedical realization, are also covered.

Keywords: ^{13}C metabolic MRI, dynamic nuclear polarization, hyperpolarization, molecular imaging, parahydrogen-induced polarization

Introduction

Hyperpolarization refers to a class of methods that enable the fundamental sensitivity limits of magnetic resonance imaging (MRI) to be overcome, allowing functional imaging of exogenous agents of unprecedented quality.¹ Over the last 20 years, hyperpolarized (HP) ^3He and ^{129}Xe noble gases have been developed from experimental tools into safe, inhalable contrast agents for high-resolution, functional MRI of the lung airspaces and are already used routinely in a clinical setting.² On the other hand, HP ^{13}C -labelled liquid-phase probes for molecular and metabolic MRI hold great promise for interrogating pathophysiology at the cellular level.³

The first *in-man* hyperpolarized $[1-^{13}\text{C}]$ pyruvate MRI exams in patients with prostate cancer realized the potential for observing metabolic processes beyond glycolysis, which is typically probed by ^{18}F -fluorodeoxyglucose positron-emission tomography (^{18}F -FDG-PET); until recently the only metabolic imaging method used routinely in the oncology clinic.⁴ This pioneering study has been followed by a rapid dissemination of HP $[1-^{13}\text{C}]$ pyruvate MRI for clinical applications,⁵ facilitated by the development of commercial, sterile polarization systems for clinical use.⁶ As of June 2019, more than 30 clinical trials worldwide pertaining to HP $[1-^{13}\text{C}]$ pyruvate MRI are either in a complete, in progress, or pending phase and this number is predicted to only increase further over the coming years.

In this review article, we provide a brief overview of the concept of hyperpolarization and the theory behind the methods to obtain liquid-state ^{13}C polarization; namely, dissolution dynamic nuclear polarization (d-DNP) and parahydrogen-induced polarization (PHIP), followed by a comprehensive review of the biomedical applications of HP ^{13}C MRI by, with a particular focus on recent clinical MRI applications of HP $[1-^{13}\text{C}]$ pyruvate and other hyperpolarized ^{13}C molecular imaging probes with clinical promise.

Division of Bioengineering and Bioinformatics, Graduate School of Information Science and Technology, Hokkaido University, Hokkaido, Japan

*Corresponding author: Division of Bioengineering and Bioinformatics, Graduate School of Information Science and Technology, Hokkaido University, Sapporo 060-0814, Hokkaido, Japan. Phone: +81-11-706-6789, Fax: +81-11-706-6802, E-mail: smatsumoto@ist.hokudai.ac.jp

©2019 Japanese Society for Magnetic Resonance in Medicine
This work is licensed under a Creative Commons Attribution-NonCommercial-NoDerivatives International License.

Received: August 21, 2019 | Accepted: November 4, 2019

Theoretical Background

Hyperpolarization

When placed in a magnetic field B_0 , spin- $\frac{1}{2}$ nuclei of gyromagnetic ratio γ occupy one of two Zeeman states at energies $\pm\gamma\hbar B_0/2$. The nuclear spin “polarization” is defined as the fractional difference in the population of the two states, which under conditions of thermal equilibrium is derived from the Boltzmann distribution:

$$P = \tan h \left(\frac{\Delta E}{2k_B T} \right) \approx \left(\frac{\gamma\hbar B_0}{2k_B T} \right) \quad (1)$$

The Boltzmann (thermal) polarization of ^{13}C —the only stable spin- $\frac{1}{2}$ carbon nucleus—at typical clinical magnetic field strengths is $\sim 10^{-6}$. In fact, MR of endogenous ^{13}C is challenging not just due to its \sim fourfold lower gyromagnetic ratio than ^1H ; the natural abundance of ^{13}C is only 1.1% and thus sensitivity is poor. A ~ 100 -fold MR signal enhancement can be obtained on endogenous tracers through ^{13}C -labeling, and a further 4–5 orders of magnitude enhancement via hyperpolarization.

Hyperpolarization denotes a temporary state of dramatic population excess in one nuclear spin state (see Fig. 1) and can be realized by a number of approaches; brute force polarization (utilizing low temperatures and high magnetic fields to directly increase the nuclear polarization)^{7,8}; spin-exchange optical pumping⁹ and metastability-exchange optical pumping¹⁰ for hyperpolarized gases; and d-DNP¹¹ and PHIP¹² for solution-state ^{13}C applications. The latter two methods have been demonstrated for biomedical ^{13}C molecular MRI

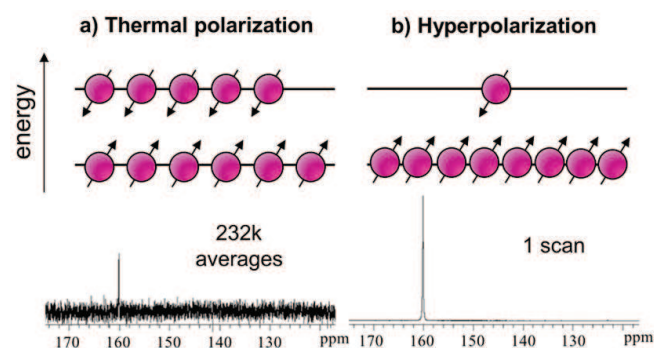


Fig. 1 Concept of hyperpolarization. (a) The occupation of nuclear Zeeman states of a spin- $\frac{1}{2}$ system in thermal equilibrium in a magnetic field follows that of the Boltzmann distribution [cf. Equation (1)]; for ^{13}C at 1.5T and 300 K, the polarization, i.e. the population difference between the spin up and down states for ^{13}C is only $P \sim 10^{-6}$. (b) Hyperpolarization describes the state of a large excess population in one of the nuclear Zeeman states, leading to a nuclear polarization several orders of magnitude greater than the Boltzmann polarization (Data is reproduced from the original dissolution dynamic nuclear polarization (d-DNP) paper¹¹ (Copyright (2003) National Academy of Sciences, USA) and compares NMR spectra obtained from thermally-polarized and hyperpolarized ^{13}C urea of ~ 60 mM concentration).

applications and these form the focus of this review article. We note that signal amplification by reversible exchange (SABRE),¹³ closely-related to conventional PHIP, is recently showing progress toward potential *in vivo* application¹⁴ but will not be covered in this article as biomedical application is yet to be shown; we refer the reader to Robertson and Mewis¹⁵ for an up-to-date review.

The MR signal enhancement associated with hyperpolarization is not permanent; longitudinal relaxation acts to return the nuclear spin state populations to that of thermal equilibrium, and after radiofrequency excitation, the hyperpolarized state is not recovered.¹⁶ Research into generating so-called “long-lived” states and also generation of continuously re-hyperpolarization¹⁷ are an active fields¹⁸; however, hyperpolarized $[1-^{13}\text{C}]$ pyruvate, the most promising molecule for clinical applications, remains limited by a $T_1 \sim 60$ s. The decay in magnetization associated with a number of RF excitations n with repetition time TR and flip angle α can be described as follows:

$$M_{xy}(n) = M_0 \exp \left[-(n-1) \frac{TR}{T_1} \right] \sin(\alpha_n) \prod_{j=1}^{n-1} \cos(\alpha_j) \quad (2)$$

For a constant flip angle, and $TR \ll T_1$, Equation (2) can be simplified to $M_{xy}(n) = M_0 \sin(\alpha) \cos^{n-1}(\alpha)$ [for example, after $N = 128$ RF excitations at flip angle 8° a magnetization of only $M_{xy}(N) \approx 0.3M_0 \sin(8^\circ)$ remains]. The signal decay during acquisition leads to filtering of the k -space and image blurring, but which can be somewhat compensated for by modifying the flip angle throughout the acquisition process.^{16,19} Nevertheless, acquisition of hyperpolarized signals necessitates efficient encoding of k -space, such as with spiral trajectories,²⁰ parallel imaging²¹ or compressed sensing.²² Hyperpolarized ^{13}C metabolic MRI relies upon the discrimination of MR signals from the injected probe (e.g. pyruvate) and its metabolic products (e.g. lactate) by chemical shift. If spatial information is not essential, dynamic spectroscopy is a simple and robust means to probe metabolism dynamics.²³ Several imaging strategies have been developed²⁴ including: phase-encoded chemical shift imaging (CSI)²⁵ which although inefficient, allows acquisition of full spectra; echo planar spectroscopic imaging, in which (usually fly-back) gradients are used for simultaneous 1D spatial encoding and spectral readout, permitting several-fold acceleration at the expense of SNR;^{26,27} spiral chemical shift imaging, wherein multi-dimensional spatial data is encoded simultaneously with spectral data in a similar manner to tomosynthesis;²⁸ spiral encoding schemes²⁹ combined with the robust iterative decomposition with echo asymmetry and least-squares estimation technique;³⁰ and spectral-spatial excitation for additional efficiency and the flexibility of a different flip angle on each resonance of interest.³¹ In light of the long T_2 of ^{13}C *in vivo*, SNR benefits have been realized by using single or multi-echo balanced steady-state free precession.^{32,33}

Dynamic nuclear polarization

Dissolution dynamic nuclear polarization—to date the principal polarization techniques employed to generate hyperpolarized $[1-^{13}\text{C}]$ pyruvate—relies upon the relatively large electron gyromagnetic ratio ($\gamma_e \approx 660\gamma_p$) which [according to Equation (1)] leads to an electron Boltzmann polarization of approximately unity at temperatures ~ 1 K at high field (see Fig. 2a).³⁴ An efficient electron paramagnetic agent (free radical, see e.g. Lumata et al.³⁵) is mixed with a glassing agent and the target probe to be polarized (e.g. pyruvate), which is cooled to ~ 1 K under a magnetic field of several tesla. In the subsequent glassy solid state where d-DNP is most efficient, microwave irradiation is used to induce polarization transfer from free electrons to ^{13}C nuclei over the course of ~ 1 h. At temperatures < 4.2 K, polarization transfer is believed to be primarily driven by the thermal mixing effect,³⁶ though depending on exact experimental conditions, contributions from the so-called solid effect and cross effect,³⁷ and the Overhauser effect in the solution phase,³⁸ may not be ignored. After polarization transfer, the frozen

sample is rapidly dissolved in a superheated solvent and transferred to the MRI system for measurement [hence the term “dissolution (d)”¹¹].

The first commercial d-DNP system for preclinical research applications shortly followed the publication of the original d-DNP paper¹¹ (HyperSense, Oxford Instruments, UK) and other efficient research systems have since been developed.³⁹ Most d-DNP systems including the HyperSense require large quantities of liquid helium to maintain the low sample temperature; however, two recent landmark developments have enabled d-DNP without consumption of cryogenics; a high-throughput, sterile polarizer for clinical applications SpinLab⁶ (GE Healthcare, Waukesha, WI, USA), and an efficient research polarizer with variable magnetic field (the SpinAligner, (Polarize, Frederiksberg, Denmark)),⁴⁰ both of which are commercially available. The SpinLab (Fig. 2a), operating at ~ 0.9 K and 5T and routinely obtaining up to 40% $[1-^{13}\text{C}]$ pyruvate polarization, is the only system to date approved for human application.

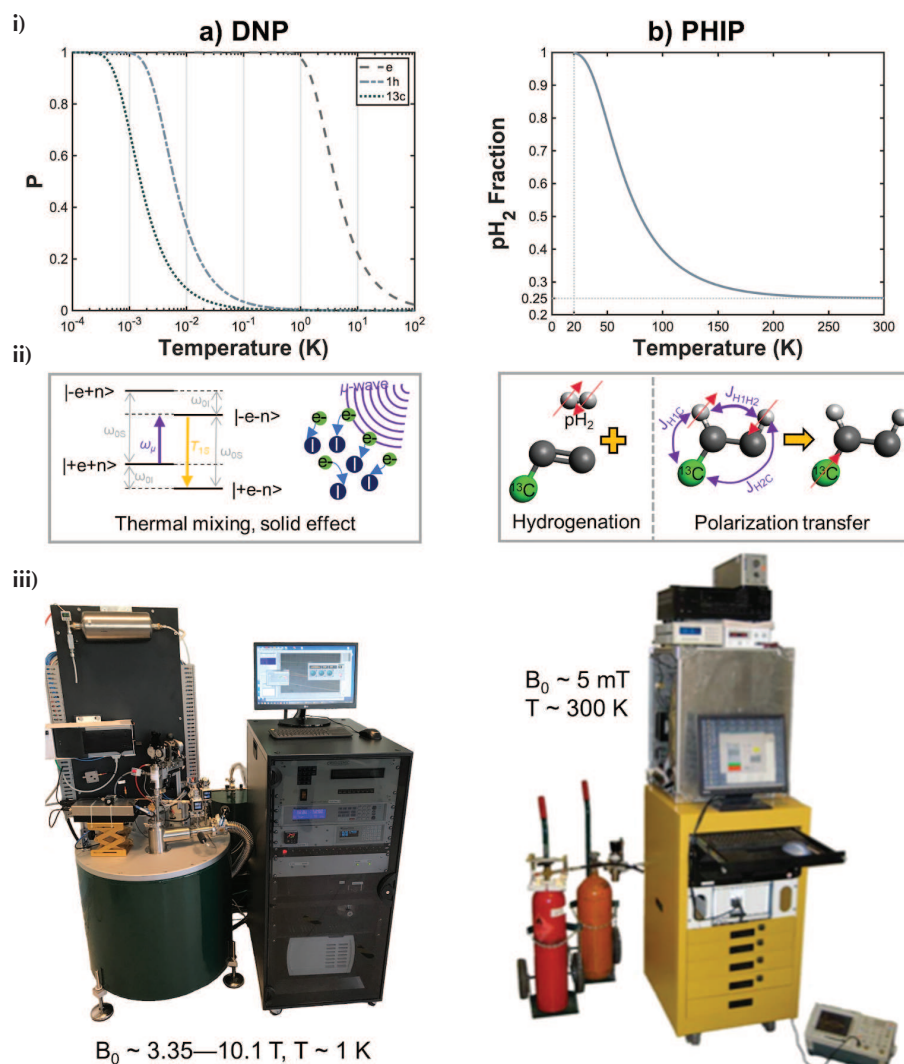


Fig. 2 Concept diagram for dissolution dynamic nuclear polarization (d-DNP) and parahydrogen-induced polarization (PHIP) polarization techniques. **(a)** In d-DNP, the source of ^{13}C nuclear polarization (P) is the approximately unity electron polarization (P) at low temperature and high magnetic field (curves plotted for 3.35T) (i). This is transferred to ^{13}C via microwave excitation (ii), predominantly mediated via the thermal mixing effect. (iii) Prototype commercial cryogen-free d-DNP system reported in Ardenkjaer-Larsen et al.⁴⁰ (original photo courtesy of Jan Henrik Ardenkjaer-Larsen, Technical University of Denmark and GE Healthcare). **(b)** In PHIP, the source of ^{13}C polarization is the inherent spin order of the parahydrogen polarization (P) at very high purity by cooling normal hydrogen in the presence of a paramagnetic catalyst (i). Parahydrogen is reacted with an unsaturated substrate, generating ^1H hyperpolarization, which is subsequently transferred to ^{13}C or other target heteronucleus (ii). Several dedicated low-field (mT) polarization systems have been designed for automating the hydrogenation and polarization transfer processes; the example shown is reprinted with permission from Springer Nature (Hövenner et al.).⁵⁸

Parahydrogen-induced polarization

Despite surmounting the hurdle associated with cryogen consumption, the initial outlay required for d-DNP systems remains high (~several million USD for the SpinLab). PHIP¹² is a relatively recent technique that offers a cheaper route to hyperpolarized ¹³C molecules for biomedical MRI applications.⁴¹ PHIP relies on the inherent spin order of parahydrogen, a spin isomer of hydrogen. At room temperature, the two spin- $\frac{1}{2}$ nuclei of each hydrogen molecule have an equal probability to occupy one of four spin states; three states of total spin 1 (orthohydrogen, “triplet” state) and one state of total spin 0 (parahydrogen, “singlet” state). When cooled in the presence of a paramagnetic catalyst (typically iron(III) oxide or charcoal, which promotes the otherwise slow symmetry-forbidden transition between orthohydrogen and the lower energy parahydrogen state) to ~20 K, a parahydrogen fraction of ~1 can be obtained (see Fig. 2b).

Parahydrogen itself is NMR silent since it has a total nuclear spin of 0; however, upon pairwise addition to magnetically-inequivalent sites on an unsaturated substrate molecule, the symmetry of the parahydrogen singlet state is broken and hyperpolarized ¹H MR signals can be observed. This hydrogenation reaction is typically performed in an organic solvent or the aqueous phase in the presence of a transition metal (typically Rh- or Ru-)based catalyst.⁴² The resulting ¹H nuclear spin state depends on the magnetic field at which parahydrogen addition is performed; at high field, e.g. within the MR system itself, the parahydrogen and synthesis allow dramatically enhanced nuclear alignment effect is observed,¹² whilst for hydrogenation at low field followed by adiabatic transport of the sample to the MR system for detection, the adiabatic longitudinal transport after dissociation engenders nuclear alignment effect is observed.⁴³ Several studies using PHIP of ¹H nuclei have been performed (e.g. to generate J-coupling derived contrast⁴⁴ and gas-phase imaging⁴⁵); however, due to the large background signal *in vivo* and lack of attainable pathophysiological functional information such as that pertaining to metabolism, heteronuclei such as ¹³C or ¹⁵N are of greater interest for biomedical applications. Polarization transfer from ¹H to heteronuclei is mediated by spin–spin couplings and can be driven by specialized RF pulse sequences^{46–48} or by subjecting the sample to a magnetic field cycle.^{49–51} The selection of polarization transfer method and its parameters depends on the configuration of the target molecular probe.^{52,53}

Regarding hardware, parahydrogen enrichment of ~50% can be achieved by simply flowing hydrogen gas through a cryogenic tube submersed in liquid nitrogen.⁵⁴ A high-throughput system to generate and store up to 50 bar of 98% parahydrogen has been developed for biomedical applications⁵⁵; once stored, parahydrogen enrichment can be maintained for months provided that paramagnetic molecular oxygen is not present.⁵⁶ Several automated PHIP polarizers for low-field hydrogenation and polarization transfer have been developed^{57–59} incorporating heated, high-pressure

spray reactors; however, promising results have also been obtained by simply shaking or bubbling of a parahydrogen-filled NMR tube followed by field cycling by hand (see e.g. Chukanov et al.⁶⁰). In addition, unlike d-DNP, it is possible to perform both the hydrogenation reaction and polarization transfer and generate heteronuclear hyperpolarization within the NMR magnet itself, minimizing the time for polarization decay.^{46,61}

d-DNP-polarized [1-¹³C]pyruvate: the pathway to clinical application

Abnormal metabolism is a hallmark of cancer, cardiovascular disease and other pathologies, and is intrinsically linked to inflammation and immune response.⁶² ¹⁸F fluorodeoxyglucose (FDG), a glucose analog, is routinely used for high-sensitivity and specificity clinical PET imaging of glucose metabolism⁶³ and is the recommended clinical indicator for head, neck, lung and pancreatic cancer.⁶⁴ However, since FDG-6-phosphate does not undergo further glycolysis, FDG-PET cannot probe metabolism beyond the first step of the glycolysis pathway. In this respect, d-DNP of [1-¹³C]pyruvate represents a significant development permitting unprecedented access to downstream metabolites to further aid understanding of cancer and disease mechanisms.

Whilst the first *in vivo* studies of a molecule polarization by d-DNP were performed with HP ¹³C-urea,⁶⁵ it was quickly realized that [1-¹³C]pyruvate, which plays a critical role in metabolism (see Fig. 3), is an ideal molecule for d-DNP since it is self-glassy and has long T₁ for ¹³C at the 1 and 2 positions (~40–60 s).⁶⁶ Golman et al.⁶⁷ demonstrated the first real-time metabolic imaging of metabolic production of [1-¹³C]lactate, [1-¹³C]alanine and [1-¹³C]bicarbonate from hyperpolarized [1-¹³C]pyruvate in healthy rats and pigs, and demonstrated differences in metabolite signal intensity in tumor tissues.⁶⁸ In cancer cells, glycolysis prevails over oxidative phosphorylation and the conversion of pyruvate to lactate via lactate dehydrogenase is up-regulated; this is known as the Warburg effect.⁶⁹ To date, increased HP [1-¹³C]pyruvate to [1-¹³C]lactate conversion has been used as the principal outcome of HP [1-¹³C]pyruvate MRI studies in several types of cancers.^{68,70–73} The high sensitivity of HP [1-¹³C]pyruvate MRI affords the possibility of non-invasive assessment of cancer treatment response, first demonstrated by Day et al.,⁷⁴ who showed a decrease in of HP ¹³C pyruvate–lactate flux after chemotherapy. The technique has since been applied in several studies of radiotherapy response^{75,76} and assessment of other treatments^{77,78} and reported to present a viable clinical alternative to FDG-PET for early tumor response in a preclinical study.⁷⁹

In a landmark paper, Nelson et al. reported the utilization of GE’s prototype sterile d-DNP system⁶ to perform the first *in-man* HP [1-¹³C]pyruvate MR spectroscopy and imaging feasibility study of patients with prostate cancer,⁴ demonstrating distinction of high- and low-grade tumors. This development has opened the door to realize real-time clinical metabolic imaging with HP [1-¹³C]pyruvate and the rapid

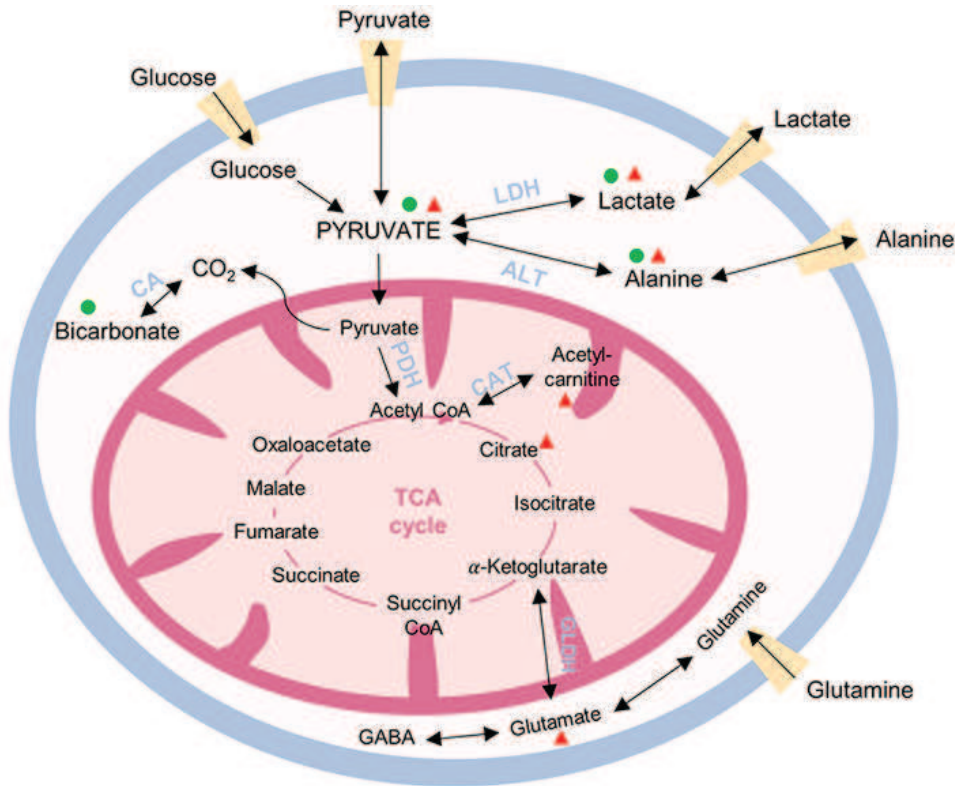


Fig. 3 Schematic of glycolysis, pyruvate metabolism to alanine and lactate, and the tricarboxylic acid (TCA) cycle within the mitochondria. Green circles: products of [1-¹³C]pyruvate; red triangles: products of [2-¹³C]pyruvate.

uptake of the technology is epitomized by the fact that more than 20 GE SpinLab polarizers have been installed worldwide, with close to half presently in use for human studies. First reports of the application of [1-¹³C]pyruvate to study metabolism in the healthy human heart⁸⁰ and brain⁸¹ have reported good tolerance of the procedure and contributed valuable reference data for interpretation of patient studies. In prostate cancer, HP [1-¹³C]pyruvate has been shown to detect early response to androgen deprivation therapy with a sensitivity exceeding that of T₂- and diffusion-weighted MRI.⁸² Preliminary reports in patients with liver metastases⁸³ and those with brain tumors^{84,85} demonstrate the wide range of potential targets of the technology and provide important pilot data for future trials. Several of these early clinical results are summarized in Fig. 4. Furthermore, at the 2019 International Society for Magnetic Resonance in Medicine (ISMRM) meeting, first HP [1-¹³C]pyruvate data in human patients with breast cancer, in which the relationship between intertumoral heterogeneity and gene expression analysis was investigated,⁸⁶ and preliminary *longitudinal* HP [1-¹³C]pyruvate data in glioma patients^{87,88} was reported, highlighting the advantages of the non-invasive nature of the technique for short- and long-term patient follow-up. Moreover, more than 30 clinical trials (sum of completed, ongoing and pending trials) are registered on the US and European clinical trials registries (summarized in Table 1) targeting a range of conditions, including prostate, brain, breast, ovarian, uterine, pancreatic and skin cancers, in addition to cardiovascular

indications and other brain pathologies. Comparison with FDG-PET to further comprehend the complementary information that can be obtained^{89,90} is a critical next step to aid interpretation of human HP [1-¹³C]pyruvate data and encourage further clinical dissemination.

As the number of clinical studies with [1-¹³C]pyruvate increases, there is a growing need for robust quantitation methods that can be applied universally for multi-site validation studies.⁹¹ Typically, HP [1-¹³C]pyruvate MR examinations include dynamic spectroscopy of the time-course of metabolic conversion of pyruvate, in addition to imaging. Semi-quantitative analysis of metabolic dynamics measured by MR spectroscopy can be performed using one of several models that have been developed to describe the rate of pyruvate–lactate conversion k_{PL} .⁹² For the most simple two-compartment model of pyruvate–lactate conversion, written in matrix form (see e.g. Harrison et al.⁹² and Harris et al.⁹³):

$$\frac{d}{dt} \begin{bmatrix} P_z \\ L_z \end{bmatrix} = \begin{bmatrix} -k_{PL} - \rho_P & k_{LP} \\ k_{PL} & -k_{LP} - \rho_L \end{bmatrix} \begin{bmatrix} P_z \\ L_z \end{bmatrix} \quad (3)$$

where P_z and L_z are the z-magnetization of pyruvate and lactate, respectively, k_{LP} is the (reverse) lactate–pyruvate conversion rate and $\rho_i = 1/T_{1,i} - \log(\cos(\alpha))/TR$ describes T₁ relaxation and RF-induced depolarization [cf. Equation (2)]. This equation can be analytically⁷⁴ or numerically solved and utilized to fit the magnetic resonance spectroscopy

(MRS) signal intensities of lactate and pyruvate (see for example the data in Fig. 4a) to yield k_{PL} as a metric of the Warburg effect. Model-free approaches such as the area under the signal-time curve and time-to-peak present simple, robust alternatives.⁹¹ CSI-based techniques yield individual images for each metabolic product, and ratio maps of lactate to pyruvate signal intensity are commonly used to provide some degree of quantitation in a regional manner.

d-DNP beyond [1-¹³C]pyruvate: other candidate molecular probes

The range of molecular imaging targets that can be polarized by d-DNP is vast and an exhaustive list⁹⁴ is beyond the scope of the present article. In the following, we introduce several of the most promising d-DNP-polarizable ¹³C molecular probes for biomedical applications (see Table 2 for a summary).

While the large majority of pre-clinical and clinical studies to date have exploited the sensitivity of HP [1-¹³C] pyruvate to the Warburg effect (i.e. pyruvate–lactate metabolism), the C₁ atom of the remaining pyruvate that enters into the mitochondria is oxidized to CO₂ and subsequently converted to bicarbonate, and thus cannot be used to probe tricarboxylic acid (TCA) cycle metabolism. However, the C₂ atom passes to acetyl-CoA and enters into the TCA cycle, exhibiting several metabolic fates (Figs. 3 and 5b). Schroeder et al.²³ first reported detection of downstream metabolites including [1-¹³C]acetylcarnitine, [1-¹³C]citrate, [5-¹³C]glutamate in perfused rat hearts after injection of HP [2-¹³C]pyruvate, with decreased citrate and glutamate production post-ischemia. In response to rapid pacing challenge, *in vivo* measurements of cardiac metabolism showed increased [5-¹³C]glutamate production,⁹⁵ and increased glutamate,

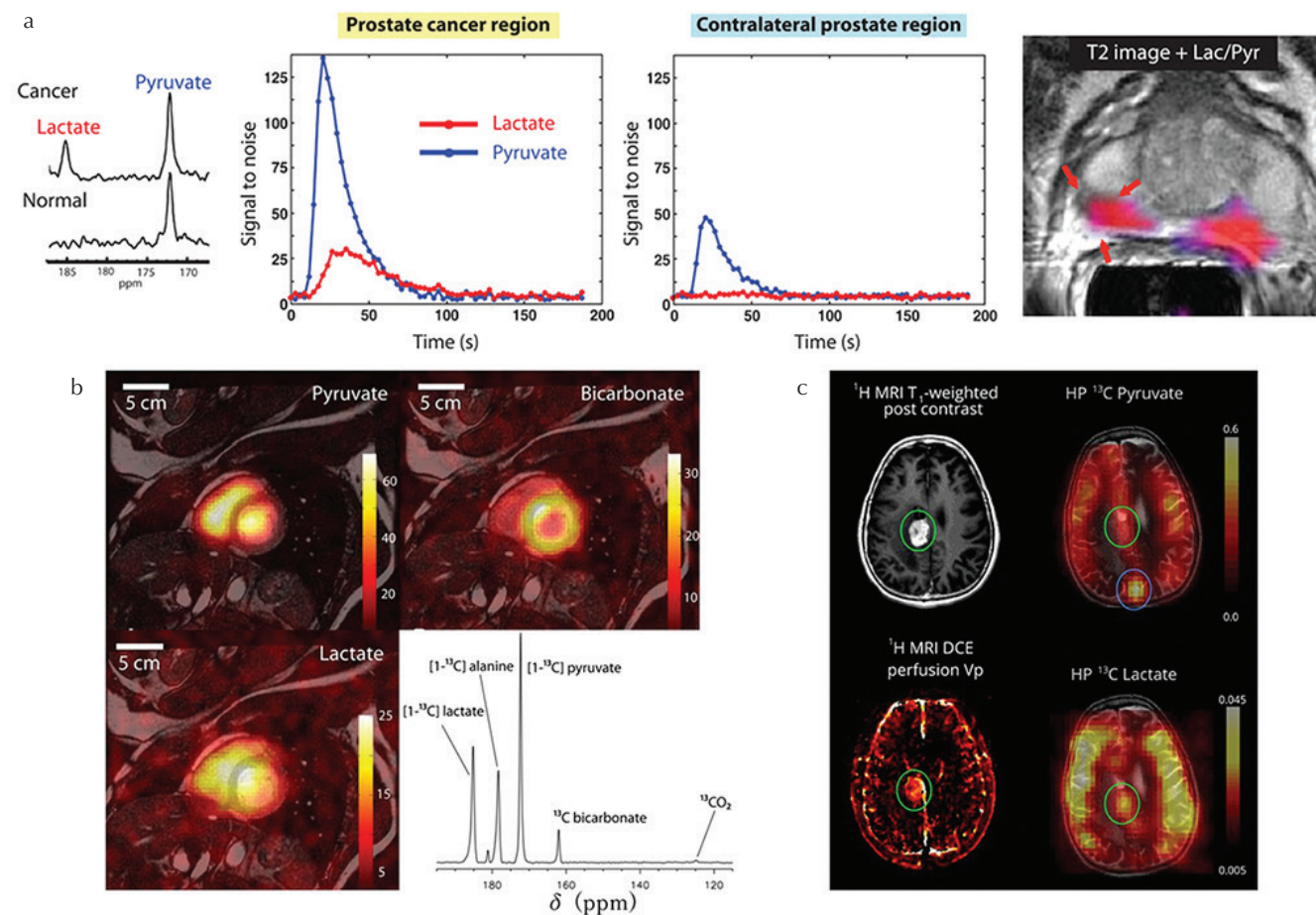


Fig. 4 Clinical examples of hyperpolarized [1-¹³C]pyruvate MRI. (a) Representative dynamic ¹³C MRS data of pyruvate and lactate signal in prostate cancer region and contralateral prostate region of a prostate cancer patient, and lactate/pyruvate signal ratio map overlaid on a T₂-weighted ¹H MR image (adapted from Figs. 2 and 4, respectively of Nelson et al.⁴ reprinted with permission from the American Association for the Advancement of Science (AAAS)). (b) HP [1-¹³C]pyruvate, lactate and bicarbonate MR images and a non-selective MR spectrum of the healthy human heart (adapted from Figs. 1 and 3, respectively of Cunningham et al.⁸⁰ reprinted with permission from Wolters Kluwer Health, Inc). (c) Comparison of HP [1-¹³C]pyruvate and lactate MR images to contrast-enhanced T₁-weighted MRI and perfusion plasma volume mapping in a patient with recurrent glioblastoma (adapted from Fig. 4 of Miloshev et al.⁸⁵ permission from the American Association for Cancer Research (AACR)).

Table 1 Summary of ongoing clinical trials pertaining to hyperpolarized ¹³C MRI (from clinicaltrials.gov, clinicaltrialsregister.eu and drks.de, accessed on 2019/06/12)

Primary condition (number of trials)	Participating center (country)	Enrollment [†]
Brain cancer ⁶	Sunnybrook Health Sciences Centre, Toronto (Canada)	121
	UT Southwestern Medical Center, Dallas (USA)	44
	M D Anderson Cancer Center, Dallas (USA)	13
	University of California San Francisco, San Francisco (USA)	80
	UCSF Helen Diller Family Comprehensive Cancer Center, San Francisco (USA)	9
Uterine and ovarian cancer ²	Sunnybrook Health Sciences Centre, Toronto (Canada)	10
	Addenbrooke's Hospital, Cambridge (UK)	40
Breast cancer ²	UT Southwestern - Advanced Imaging Research Center, Dallas (USA)	110
	Sunnybrook Health Sciences Centre, Toronto (Canada)	13
Traumatic brain injury and CNS tumors ²	UT Southwestern Medical Center, Dallas (USA)	16
	Stanford University School of Medicine, Palo Alto (USA)	10
Other: Sarcoma ¹	Advanced Imaging Research Center, Dallas (USA)	20
Fatty liver ¹	UT Southwestern Medical Center, Dallas (USA)	16
Pancreatic cancer ¹	Aarhus University Hospital, Aarhus (Denmark)	15
Skin cancer ¹	Aarhus University Hospital, Aarhus (Denmark)	30
General cancer ¹	Memorial Sloan Kettering Cancer Center, New York (USA)	84
Prostate cancer ⁹	University of California San Francisco, San Francisco (USA)	261
	Sunnybrook Health Sciences Centre, Toronto (Canada)	40
	M D Anderson Cancer Center, Dallas (USA)	10
	University of California San Francisco, San Francisco (USA)	261
Cardiovascular disease ⁵	UT Southwestern Medical Center, Dallas (USA)	10
	Sunnybrook Health Sciences Centre, Toronto (Canada)	112
	University College London, London (UK)	25
	University Hospital Zurich, Zurich (Switzerland)	50
	Aarhus University Hospital, Aarhus (Denmark)	20

[†]Enrollment: approximate patient numbers scanned or anticipated (in cases of multiple studies at the same center, enrollment represents a summation of the enrollment for each individual study).

Table 2 Non-exhaustive list of ¹³C MR molecular probes polarizable by dynamic nuclear polarization (adapted with the publisher's permission from Table 1 of Hurd et al.¹⁶³) and their chemical shift (and literature reference)

HP ¹³ C probe (chemical shift)	Metabolic products (chemical shift)	Biomedical applications
[1- ¹³ C]Pyruvate (173 ppm) ¹⁶⁴	[1- ¹³ C]Lactate (185 ppm), [1- ¹³ C]alanine (178 ppm), [1- ¹³ C]bicarbonate (162 ppm), [1- ¹³ C]pyruvate hydrate (181 ppm) ¹⁶⁴	Warburg effect (cancer)
[2- ¹³ C]Pyruvate (208 ppm) ⁹⁶	[2- ¹³ C]Lactate (71 ppm), ⁹⁶ [2- ¹³ C]alanine (53 ppm), [1- ¹³ C]citrate (180–181 ppm), ¹⁶⁵ [5- ¹³ C]glutamate (184 ppm), [1- ¹³ C]acetylcarnitine (175 ppm), [3- ¹³ C]acetoacetate (177 ppm) ⁹⁶	Tricarboxylic acid (TCA) cycle metabolism
¹³ C-Urea (162.5 ppm) ¹⁰⁰	None (end product)	Perfusion
[1,4- ¹³ C ₂]Fumarate (175.4 ppm) ¹⁰³	[1- ¹³ C]Malate (181.8 ppm), [4- ¹³ C]Malate (180.6 ppm) ¹⁰³	Cellular necrosis
[1- ¹³ C] Dehydroascorbate (174.0 ppm) ¹⁰⁹	[1- ¹³ C]Ascorbic acid (vitamin C) (177.8 ppm) ¹⁰⁹	Redox status
¹³ C-Bicarbonate (161 ppm) ¹¹³	Carbon dioxide (125 ppm) ¹¹³	pH mapping
[1,5- ¹³ C ₂]Zymonic acid (ppm _{urea} + 10–15 ppm) ^{116*}	None	
[5- ¹³ C]Glutamine (178.5 ppm) ¹⁶⁶	[5- ¹³ C]Glutamate (181.5 ppm) ¹⁶⁶	Glutaminase metabolism,
[1- ¹³ C]α-ketoglutarate (172.6 ppm) ¹¹⁷	[1- ¹³ C]Glutamate (177.5 ppm) ¹¹⁷	TCA cycle metabolism
[1- ¹³ C]Acetate (182.5 ppm) ¹²⁰	[1- ¹³ C]Acetylcarnitine (202.1 ppm) ¹²⁰	Acetyl-CoA synthetase activity

*pH-dependent chemical shift.

acetoacetate and acetylcarnitine production was observed post-injection of an anti-cancer agent in rats.⁹⁶ The first clinical MR spectroscopy and imaging data of HP [2-¹³C]pyruvate in the healthy human brain was reported at the 2019 ISMRM meeting,⁹⁷ however, application of the probe remains challenging due to the relatively low concentration of downstream metabolites generated; in one study, none were detectable.⁶⁶

[1-¹³C]urea, the first hyperpolarized ¹³C molecular MR imaging agent demonstrated by the d-DNP method,¹¹ is metabolically inert and shows promise as a HP MRI agent for perfusion assessment.^{98,99} Furthermore, [1-¹³C]urea can be co-polarized with [1-¹³C]pyruvate for simultaneous assessment of metabolism and perfusion,¹⁰⁰ and co-labeling with ¹⁵N₂ exhibits prolonged ¹³C relaxation times and improved SNR¹⁰¹ facilitating for example the investigation of renal functional changes.¹⁰²

[1,4-¹³C₂]fumarate can be hyperpolarized by d-DNP and the rate of its conversion to malate, catalyzed by fumarase, is indicative of cellular necrosis.¹⁰³ HP [1,4-¹³C₂]fumarate exhibits high sensitivity to necrosis in myocardial infarction¹⁰⁴ and acute kidney injury¹⁰⁵ among other tissue pathologies, is complementary to [1-¹³C]pyruvate in the assessment of treatment response (Fig. 5a) in breast cancer¹⁰⁶ and efficient co-polarization schemes offer simultaneous probing of multiple metabolic pathways.¹⁰⁷

Hyperpolarization of the reduced and oxidized forms of vitamin C—namely [1-¹³C]dehydroascorbate and [1-¹³C]ascorbate, respectively—offers a novel means to probe intracellular redox status, a critical factor in normal and abnormal cellular function.^{108,109} High concentrations of [1-¹³C]ascorbate can be observed post-injection of [1-¹³C]dehydroascorbate, and reduced HP [1-¹³C]ascorbate signal has been utilized as an MR biomarker of renal oxidative stress.^{110,111}

Several HP ¹³C-based molecular probes have been proposed for measurement of pH,¹¹² a critical physiological factor. In particular, injection of hyperpolarized ¹³C-bicarbonate and monitoring of its conversion to ¹³CO₂ has been proposed to monitor pH¹¹³ and demonstrates sensitivity to abnormal pH in cancer¹¹³ and ischemic heart disease.¹¹⁴ An alternative method involves monitoring the HP ¹³CO₂ production from injected [1-¹³C]pyruvate.¹¹⁵ Recently, HP [1,5-¹³C₂]zymonic acid has been proposed for high-sensitivity *in vivo* pH mapping, exhibiting a pH-sensitive chemical shift and T₁ benefits over [1-¹³C]bicarbonate.¹¹⁶

To probe glutaminase and alanine transaminase metabolism, respectively, HP [5-¹³C]glutamine and [1-¹³C]glutamate have been investigated. Conversion of injected HP [1-¹³C]α-ketoglutarate to [1-¹³C]glutamate has been proposed as a potential biomarker of isocitrate dehydrogenase 1 gene mutations in glioma.¹¹⁷ Although the longitudinal relaxation of ¹³C nuclear spins in the glucose molecule is extremely short, perdeuteration has facilitated studies of glycolysis using HP [U-¹³C]glucose in cells¹¹⁸ and *in vivo*.¹¹⁹ The action of acetyl-CoA synthetase in generating acetyl-CoA—a

crucial molecule in fatty acid synthesis and TCA cycle metabolism—has been investigated with HP [1-¹³C]acetate in the heart^{120,121} and skeletal muscle.¹²²

PHIP: candidate ¹³C molecular and metabolic MRI probes

The choice of molecular probes for conventional hydrogenative PHIP is fundamentally limited by the requirement of an unsaturated precursor substrate (i.e. a molecule containing a double or triple bond to which parahydrogen is added to yield the hyperpolarized probe).¹²³ Nevertheless, a number of promising HP ¹³C probes for biomedical MR applications can be produced with a polarization level comparable to or approaching that of d-DNP. Some of these are highlighted in the following text and also in Table 3; for an exhaustive list, we refer the reader to Hövener et al.⁴¹

To date some of the most promising probes for metabolic MRI by PHIP are based on succinate and its derivatives (Fig. 6), the metabolic activity of which was introduced earlier. Hyperpolarized [1-¹³C]succinate can be generated by one of two PHIP strategies: two-step parahydrogen addition, first to [1-¹³C]acetylenedicarboxylate (ADC) to yield [1-¹³C]maleate, to which parahydrogen is added again to yield [1-¹³C]succinate¹²⁴; or by single-step parahydrogen addition to [1-¹³C]fumarate.^{125,126} The latter method offers a prolonged [1-¹³C]succinate polarization lifetime, particularly if deuterated fumarate is used, and also reduces the risk of undesired injection of ADC, which is mildly toxic, and also the intermediate (maleate).¹²⁵ Whilst initial *in vivo* experiments in the rat brain did not exhibit clear metabolic conversion of PHIP-polarized [1-¹³C]succinate,¹²⁴ the second hydrogenation approach enabled detection of downstream TCA cycle metabolites in a murine tumor model.¹²⁶ Furthermore, the diethyl ester of [1-¹³C]succinate, derived by parahydrogen addition of diethyl[1-¹³C]fumarate, appears to exhibit some TCA cycle metabolic sensitivity and was shown to distinguish murine tumor characteristics.^{126,127}

Hyperpolarized hydroxyethyl [1-¹³C]propionate, produced by parahydrogen addition of hydroxyethyl[1-¹³C]acrylate (HEA), presents a potential high-sensitivity PHIP contrast agent for angiography applications.^{50,128,129} In a recent study, the entire process of parahydrogen addition to HEA followed by polarization transfer, injection and *in vivo* MRI detection of HEP was realized within an MRI system, i.e. without the requirement of an external polarizer.¹³⁰ Since 2-hydroxyethyl[1-¹³C]propionate is easily polarized by PHIP and has strong, well-defined heteronuclear spin-spin couplings, it has also been utilized to validate several novel techniques for optimization of polarization transfer between parahydrogen and ¹³C.^{50,131,132}

Hyperpolarized tetrafluoropropyl[1-¹³C]propionate (TFPP) can be derived parahydrogen addition of the corresponding acrylate precursor and subsequent polarization transfer, and has been proposed as a “targeted” molecular agent for interrogating lipid-rich atherosclerotic plaques.¹³³ However, whilst HP ¹³C-HEP and ¹³C-succinate can be generated in the

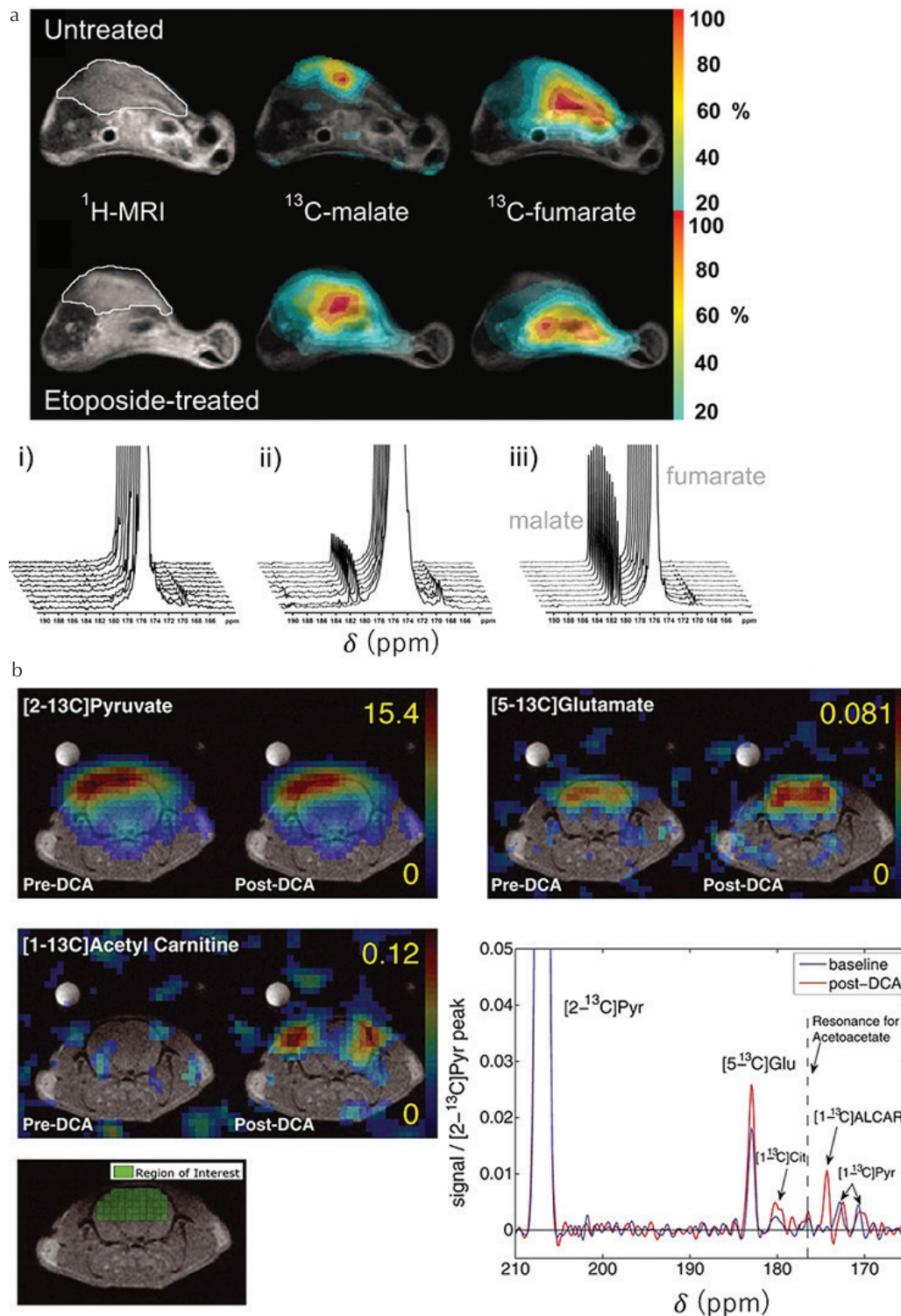


Fig. 5 Pre-clinical MRI examples of promising HP ^{13}C probes other than $[1-^{13}\text{C}]$ pyruvate. (a) HP ^{13}C chemical shift imaging (CSI) of cellular necrosis pre- and post-etoposide treatment (increased necrosis) in a murine tumor model after HP $[1,4-^{13}\text{C}_2]$ fumarate injection, and ^{13}C MR spectra obtained from murine lymphoma cells; (i) untreated, (ii) post-etoposide treatment, (iii) lysed cells, demonstrating a strong relationship between malate production and necrosis (adapted from Figs. 1 and 4 of Gallagher et al.¹⁰³ with the publisher's permission). (b) CSI-derived maps and accompanying spectra of metabolites derived from mitochondrial metabolism after injection of $[2-^{13}\text{C}]$ pyruvate into a healthy rat, exhibiting $[1-^{13}\text{C}]$ acetyl carnitine and tricarboxylic acid (TCA) cycle-derived $[5-^{13}\text{C}]$ glutamate resonances (adapted with the publisher's permission from Park et al.¹⁶⁷). Results obtained pre- and post-injection of dichloroacetate (DCA), a proposed anti-cancer drug used to influence acetyl-CoA production by modulating pyruvate dehydrogenase, are shown.

Table 3 Non-exhaustive list of ^{13}C MR molecular probes polarizable by parahydrogen-induced polarization (adapted with the publisher's permission from Table 1 of Hövener et al.⁴¹ and their chemical shift (and literature reference[†])

HP ^{13}C precursor	Hydrogenation products	Biomedical applications
[1- ^{13}C]Acetyl dicarboxylic acid (151.6 ppm) ¹⁵⁵	[1- ^{13}C]Maleate (160 ppm) \rightarrow [1- ^{13}C]Succinate (175 ppm) ¹²⁴	Tricarboxylic acid (TCA) cycle metabolism
[1- ^{13}C]Fumarate (166.5 ppm) ¹⁵⁵	[1- ^{13}C]Succinate (175 ppm) ¹²⁴	
Diethyl[1- ^{13}C]fumarate (167.4 ppm) ¹²⁷	Diethyl[1- ^{13}C]succinate (175.8 ppm) ¹²⁷	TCA cycle metabolism
^{13}C -Hydroxyethyl-acrylate	^{13}C -Hydroxyethylpropionate (~180 ppm) ⁵⁰	Angiography
Tetrafluoropropyl[1- ^{13}C]acrylate	Tetrafluoropropyl[1- ^{13}C]propionate (174 and 177 ppm) ¹³³	Atheromatous plaques
[1- ^{13}C]Phosphoenol-pyruvate (171.9 ppm) ¹³⁵	[1- ^{13}C]Phospholactate \rightarrow [1- ^{13}C]Lactate (182.1 ppm) ¹³⁵	Gluconeogenesis, lactate dehydrogenase metabolism
Propargyl[1- ^{13}C]pyruvate (160 ppm) ⁶⁰	Allyl[1- ^{13}C]pyruvate (160.5 ppm) ⁶⁰ \rightarrow [1- ^{13}C]pyruvate (173 ppm) after hydrolysis	Warburg effect (cancer)
Vinyl[1- ^{13}C]acetate (168 ppm) ⁶⁰	Ethyl[1- ^{13}C]acetate (174 ppm) ¹⁴⁷ \rightarrow [1- ^{13}C]acetate (182.5 ppm) after hydrolysis	Acetyl-CoA synthetase activity

[†]Chemical shift values only quoted for the particular solvent in the literature reference cited.

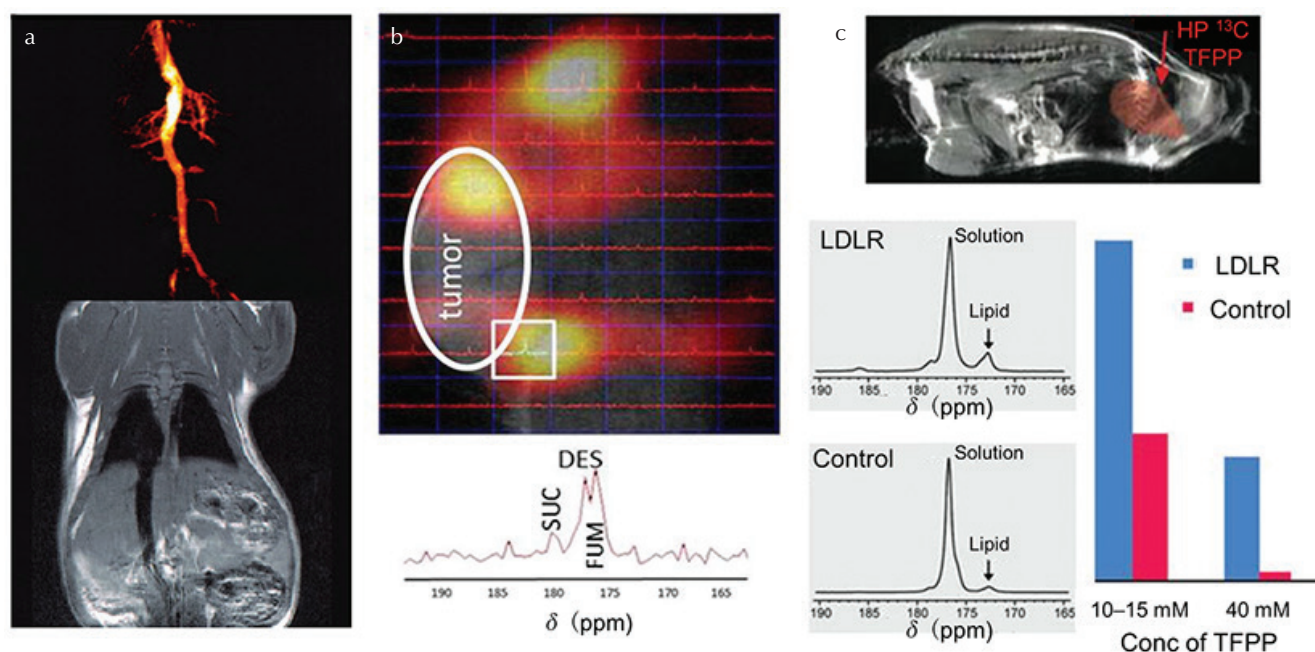


Fig. 6 *In vivo* magnetic resonance imaging (MRI) application of several hyperpolarized ^{13}C probes generated by parahydrogen-induced polarization (PHIP). (a) MRI angiogram of HP ^{13}C -labeled malate dimethyl ester with corresponding ^1H spin echo reference image of a healthy rat (adapted with permission from Golman et al.⁴⁹). (b) Chemical shift imaging (CSI) of HP diethyl [1- ^{13}C]succinate in a murine model of renal cell carcinoma (reproduced from Zacharias et al.¹²⁶ under the Creative Commons Attribution License). The ^{13}C spectrum corresponding to the pixel indicated by the white square shows tricarboxylic acid (TCA) cycle metabolism of diethyl succinate (DES) to succinate (SUC) and fumarate (FUM). (c) Representative HP tetrafluoropropyl [1- ^{13}C]propionate (TFPP) fast imaging with steady-state precession (FISP) image overlaid on a ^1H RARE image, and HP ^{13}C -TFPP spectra obtained from low density lipoprotein receptor (LDLR) deficient mice compared with control mice, demonstrating excess lipid in LDLR mice (reproduced from Bhattacharya et al.¹³³ with the publisher's permission).

pure aqueous phase using a water-soluble catalyst, TFPP requires a high dose of ethanol as a co-solvent, limiting potential *in vivo* applications.¹³³

Since [1- ^{13}C]ethyl pyruvate ester has been shown to be polarizable by d-DNP and shows some promise in comparison to [1- ^{13}C]pyruvate for functional brain imaging

applications,¹³⁴ the hydrogenation precursor [1- ^{13}C]vinyl pyruvate is an interesting potential target for PHIP, however an efficient synthesis route remains elusive.⁶⁰

Shchepin et al.¹³⁵ have proposed [1- ^{13}C]phospholactate, the hydrogenation product of [1- ^{13}C]phosphoenolpyruvate, as a possible route to HP [1- ^{13}C]lactate *in vivo*, which

is subsequently taken up by tumors and several critical organs.^{59,136} The hydrogenation reaction can relatively easily be performed in water,¹³⁷ which holds promise for future biomedical studies.

Ester derivatives of ^{13}C -glucose have been demonstrated to be polarizable by PHIP;¹³⁸ however, the short polarization lifetime ($\sim\text{s}$) must be overcome (e.g. by deuteration) to facilitate the realization of *in vivo* glycolysis measurement by PHIP of glucose derivatives and the possibility of corroboration against FDG-PET.

Alteration of choline metabolism is a hallmark of tumor progression, and several groups have investigated choline precursors as potential molecular probes for PHIP.^{139,140} Rather than ^{13}C , ^{15}N -labeling can be used; although ^{15}N possesses an intrinsically low gyromagnetic ratio and hence sensitivity compared with ^{13}C , extremely long relaxation times can be realized, enabling metabolism dynamics to be followed over the course of several minutes. In particular, the recent demonstration of 12% ^{15}N polarization with a lifetime of over 20 min on a choline derivative is of interest for *in vivo* cancer metabolism applications.¹⁴¹

Side-arm hydrogenation (PHIP-SAH): a route to HP $[1-^{13}\text{C}]$ pyruvate

The majority of the above-mentioned probes offer only limited or no metabolic information of sufficient sensitivity compared with $[1-^{13}\text{C}]$ pyruvate produced by d-DNP; however, the lack

of a suitable hydrogenation precursor of pyruvate, lactate or other metabolically-linked molecules has led Reineri et al.¹⁴² to develop the method of side-arm hydrogenation PHIP (PHIP-SAH). In PHIP-SAH, parahydrogen is added to an unsaturated ester of the molecule of choice in the organic phase, where the hydrogenation reaction is most efficient, then polarization is transferred from ^1H to the $[1-^{13}\text{C}]$ atom of the carboxylic acid of interest, and finally the ester “side-arm” is hydrolytically cleaved to yield the HP carboxylic acid of interest along with ester alcohol in the aqueous phase. Hyperpolarized $[1-^{13}\text{C}]$ pyruvate, $[1-^{13}\text{C}]$ acetate¹⁴² and $[1-^{13}\text{C}]$ lactate¹⁴³ have been demonstrated using this approach.

Following optimization of the initial experimental procedure with a view to *in vivo* application,¹⁴⁴ a ^{13}C polarization of $\sim 5\%$ on $[1-^{13}\text{C}]$ pyruvate at the time of experiment was obtained, enabling realization of the first *in vivo* metabolic MR spectroscopy and imaging in a mouse model of dilated cardiomyopathy,¹⁴⁵ the results of which are highlighted in Fig. 7. Whilst the sensitivity remains relatively low compared with that produced by d-DNP, a recent comparison of the polarization efficiency of several pyruvate and acetate precursors has provided insights into the best substrate of choice for future *in vivo* metabolic MRI applications.¹⁴⁶ In particular, hydrogenation products ethyl acetate and allyl pyruvate (hydrogenation products of vinyl acetate and propargyl pyruvate, respectively) were found to yield the highest ^{13}C polarization.¹⁴⁶ Furthermore, when a deuterated

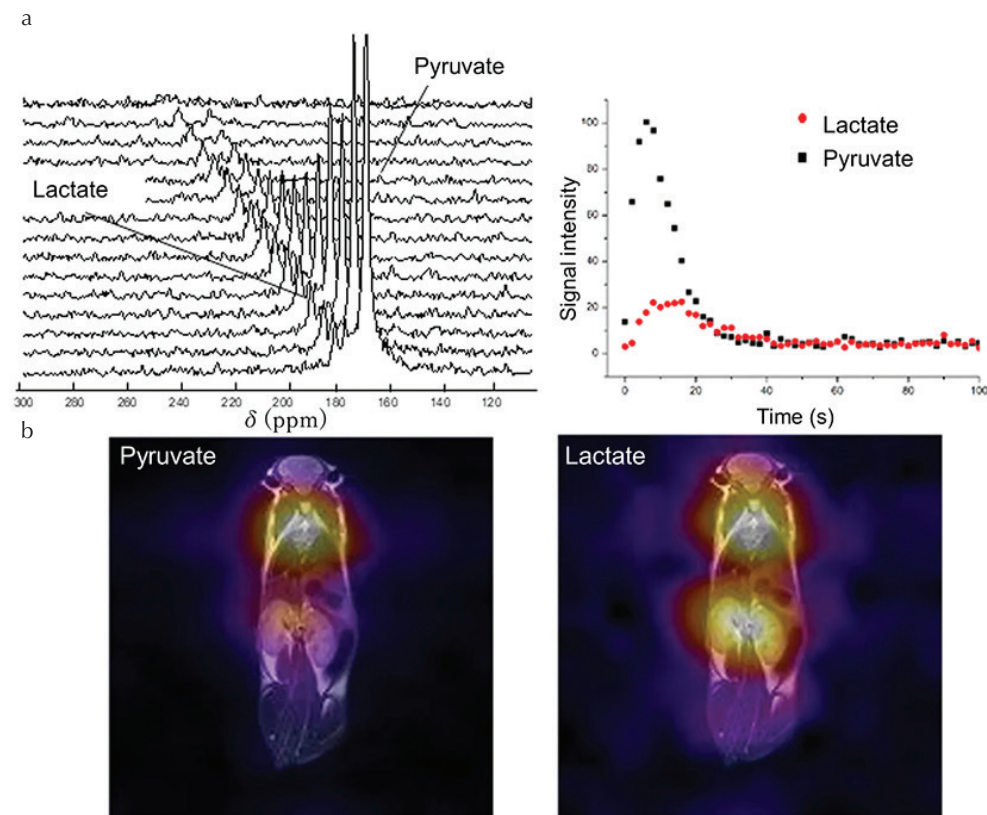


Fig. 7 (a) Slice-selective dynamic ^{13}C MRS of a healthy wild-type mouse after injection of HP $[1-^{13}\text{C}]$ pyruvate produced by parahydrogen-induced polarization (PHIP)-side-arm hydrogenation (SAH), and (b) corresponding whole-body ^{13}C chemical shift imaging (CSI) of $[1-^{13}\text{C}]$ pyruvate and $[1-^{13}\text{C}]$ lactate (reproduced from Figs. 2 and 3 of Cavallari et al.¹⁴⁵ under the Creative Commons CCBY License).

precursor is combined with optimized polarization transfer techniques, ^{13}C polarization of more than 50% on acetate has been realized using the vinyl ester precursor,¹⁴⁷ which may permit *in vivo* investigations of acetyl-CoA synthetase activity in the near future by PHIP.

Future Perspectives

Ongoing and future clinical trials of $[1-^{13}\text{C}]$ pyruvate MRI serve a critical role in evaluating the clinical viability of the technique for and beyond oncological studies of metabolism, and also in assessing the reproducibility and robustness of hyperpolarized MR acquisition methods and analysis procedures in order to provide guidelines to standardize workflow for future multi-site validation studies.⁵ In particular, robust clinical comparison studies of HP $[1-^{13}\text{C}]$ pyruvate MRI and ^{18}F -FDG-PET in several oncological pathologies are required to further understanding of the relationship between the pathophysiological information gleaned from each technique and further accelerate clinical translation.^{89,90} Clinical trials of d-DNP probes such as $[1-^{13}\text{C}]$ fumarate, $[1-^{13}\text{C}]$ bicarbonate and others are either pending or expected in the near future, and co-polarization techniques are likely to yield unprecedented access to multiple aspects of metabolic function with a single hyperpolarized dose.^{107,148} d-DNP probe development has not ceased with the advent of clinical application of $[1-^{13}\text{C}]$ pyruvate, with several novel probes reported in the last few years.^{149,151} In parallel to clinical studies, the fundamental science of d-DNP remains a field of active development.¹⁵²

Whilst biomedical applications of PHIP are relatively few in number to date when compared with those of d-DNP, novel approaches such as PHIP-SAH offer an expanded palette of polarizable molecular targets and a low-cost means of generating HP $[1-^{13}\text{C}]$ pyruvate for preclinical and with further refinement, eventually clinical applications.^{142,145} In addition, the development of increasingly efficient and versatile hydrogenation catalysts is a thriving research field (see e.g. Glöggler et al.,¹⁵³ Leutzsch et al.¹⁵⁴). In particular, rhodium-based catalysts commonly used for efficient hydrogenation predominantly yield *cis*-selective products, but a novel *trans*-selective ruthenium-based catalyst has recently been shown to demonstrate hyperpolarized $[1-^{13}\text{C}]$ fumarate by parahydrogen addition to acetylene $[1-^{13}\text{C}]$ dicarboxylate for the first time.¹⁵⁵ With appropriate filtering of the catalyst¹⁵⁶ and other unwanted co-solvents or hydrolysis side products (in the case of PHIP-SAH), the purity of injected doses can be improved to appropriately high levels with a view to clinical application in the foreseeable future.

It is not only the ^{13}C nucleus that shows promise for biomedical hyperpolarized MRI applications; as previously noted, the ^{15}N nucleus has a relatively low MR sensitivity, but exhibits extremely long polarization lifetimes and metabolic probes can be prepared in an environment suitable for biological application, analogous to ^{13}C .^{157,158} In addition, ^{19}F , which has a gyromagnetic ratio and therefore a baseline sensitivity

similar to that of the proton, may find biomedical application in targeted MRI of hyperpolarized ^{19}F -labelled drugs, though limited progress in this direction has been made to date.¹⁵⁹ Furthermore, while all the above noted applications pertain to liquid-phase molecular probes, parahydrogen can be used in combination with a solid-phase catalyst to generate ^1H -hyperpolarized propane (from propylene) in the gaseous phase.^{160,161} which shows some promise as a relatively cheap alternative to hyperpolarized noble gases for biomedical lung imaging, though the high ^1H background signal may be problematic and no *in vivo* experiments have been attempted to date.

Finally, the SABRE parahydrogen method, wherein polarization transfer occurs by reversible exchange and the target molecule remains chemically unaltered upon interaction with parahydrogen, has the potential yield heteronuclear (^{13}C , ^{15}N) hyperpolarization on a broader range of molecular imaging probes than conventional PHIP and may lead to several unprecedented avenues of biomedical application.¹⁶² Although to date no *in vivo* experiments have been performed with SABRE-polarized probes, the recent demonstration of both hyperpolarized $[1-^{13}\text{C}]$ and $[2-^{13}\text{C}]$ pyruvate,¹⁴ although at relatively low polarizations, represents a significant step toward biomedical application.

Acknowledgments

NJS is an international research fellow of the Japanese Society for the Promotion of Science (JSPS).

Conflicts of Interest

The authors declare that they have no conflicts of interest.

References

1. Nikolaou P, Goodson BM, Chekmenev EY. NMR hyperpolarization techniques for biomedicine. *Chemistry* 2015; 21:3156–3166.
2. Liu Z, Araki T, Okajima Y, Albert M, Hatabu H. Pulmonary hyperpolarized noble gas MRI: recent advances and perspectives in clinical application. *Eur J Radiol* 2014; 83:1282–1291.
3. Kovtunov KV, Pokochueva EV, Salnikov OG, et al. Hyperpolarized NMR spectroscopy: d-DNP, PHIP, and SABRE techniques. *Chem Asian J* 2018; 13:1857–1871.
4. Nelson SJ, Kurhanewicz J, Vigneron DB, et al. Metabolic imaging of patients with prostate cancer using hyperpolarized $[1-^{13}\text{C}]$ pyruvate. *Sci Transl Med* 2013; 5:198ra108.
5. Kurhanewicz J, Vigneron DB, Ardenkjaer-Larsen JH, et al. Hyperpolarized ^{13}C MRI: path to clinical translation in oncology. *Neoplasia* 2019; 21:1–16.
6. Ardenkjaer-Larsen JH, Leach AM, Clarke N, Urbahn J, Anderson D, Skloss TW. Dynamic nuclear polarization polarizer for sterile use intent. *NMR Biomed* 2011; 24:927–932.

7. Hirsch ML, Kalechofsky N, Belzer A, Rosay M, Kempf JG. Brute-force hyperpolarization for NMR and MRI. *J Am Chem Soc* 2015; 137:8428–8434.
8. Krjukov EV, O'Neill JD, Owers-Bradley JR. Brute force polarization of ¹²⁹Xe. *J Low Temp Phys* 2005; 140:397–408.
9. Walker TG, Happer W. Spin-exchange optical pumping of noble-gas nuclei. *Rev Mod Phys* 1997; 69:629–642.
10. Colegrove FD, Scheerer LD, Walters GK. Polarization of He³ gas by optical pumping. *Phys Rev* 1963; 132:2561–2572.
11. Ardenkjaer-Larsen JH, Fridlund B, Gram A, et al. Increase in signal-to-noise ratio of > 10,000 times in liquid-state NMR. *Proc Natl Acad Sci U S A* 2003; 100:10158–10163.
12. Bowers CR, Weitekamp DP. Parahydrogen and synthesis allow dramatically enhanced nuclear alignment. *J Am Chem Soc* 1987; 109:5541–5542.
13. Adams RW, Aguilar JA, Atkinson KD, et al. Reversible interactions with para-hydrogen enhance NMR sensitivity by polarization transfer. *Science* 2009;323:1708–1711.
14. Iali W, Roy SS, Tickner BJ, Ahwal F, Kennerley AJ, Duckett SB. Hyperpolarizing pyruvate through signal amplification by reversible exchange (SABRE). *Angew Chem Int Ed Engl* 2019; 58:10271–10275.
15. Robertson TBR, Mewis RE. Perspective on the hyperpolarisation technique signal amplification by reversible exchange (SABRE) in NMR spectroscopy and MR imaging. *Annu Rep NMR Spectrosc* 2018; 93:145–212.
16. Zhao L, Mulkern R, Tseng CH, et al. Gradient-echo imaging considerations for hyperpolarized ¹²⁹Xe MR. *J Magn Reson B* 1996; 113:179–183.
17. Hövener JB, Knecht S, Schwaderlapp N, Hennig J, von Elverfeldt D. Continuous re-hyperpolarization of nuclear spins using parahydrogen: theory and experiment. *Chemphyschem*. 2014; 15:2451–2457.
18. Carravetta M, Levitt MH. Long-lived nuclear spin states in high-field solution NMR. *J Am Chem Soc* 2004; 126: 6228–6229.
19. Nagashima K. Optimum pulse flip angles for multi-scan acquisition of hyperpolarized NMR and MRI. *J Magn Reson* 2008; 190:183–188.
20. Wang J, Wright AJ, Hu DE, Hesketh R, Brindle KM. Single shot three-dimensional pulse sequence for hyperpolarized ¹³C MRI. *Magn Reson Med* 2017; 77:740–752.
21. Gordon JW, Hansen RB, Shin PJ, Feng Y, Vigneron DB, Larson PEZ. 3D hyperpolarized C-13 EPI with calibrationless parallel imaging. *J Magn Reson* 2018; 289:92–99.
22. Hu S, Lustig M, Chen AP, et al. Compressed sensing for resolution enhancement of hyperpolarized ¹³C flyback 3D-MRSI. *J Magn Reson* 2008; 192:258–264.
23. Schroeder MA, Atherton HJ, Ball DR, et al. Real-time assessment of Krebs cycle metabolism using hyperpolarized ¹³C magnetic resonance spectroscopy. *FASEB J* 2009; 23:2529–2538.
24. Durst M, Koellisch U, Frank A, et al. Comparison of acquisition schemes for hyperpolarised ¹³C imaging. *NMR Biomed* 2015; 28:715–725.
25. Golman K, Petersson JS, Magnusson P, et al. Cardiac metabolism measured noninvasively by hyperpolarized ¹³C MRI. *Magn Reson Med* 2008; 59:1005–1013.
26. Yen YF, Kohler SJ, Chen AP, et al. Imaging considerations for *in vivo* ¹³C metabolic mapping using hyperpolarized ¹³C-pyruvate. *Magn Reson Med* 2009; 62:1–10.
27. Larson PE, Bok R, Kerr AB, et al. Investigation of tumor hyperpolarized [1-¹³C]-pyruvate dynamics using time-resolved multiband RF excitation echo-planar MRSI. *Magn Reson Med* 2010; 63:582–591.
28. Mayer D, Yen YF, Tropp J, Pfefferbaum A, Hurd RE, Spielman DM. Application of subsecond spiral chemical shift imaging to real-time multislice metabolic imaging of the rat *in vivo* after injection of hyperpolarized ¹³C1-pyruvate. *Magn Reson Med* 2009; 62:557–564.
29. Wiesinger F, Weidl E, Menzel MI, et al. IDEAL spiral CSI for dynamic metabolic MR imaging of hyperpolarized [1-¹³C]pyruvate. *Magn Reson Med* 2012; 68:8–16.
30. Reeder SB, Brittain JH, Grist TM, Yen YF. Least-squares chemical shift separation for (¹³)C metabolic imaging. *J Magn Reson Imaging* 2007; 26:1145–1152.
31. Schulte RF, Sperl JJ, Weidl E, et al. Saturation-recovery metabolic-exchange rate imaging with hyperpolarized [1-¹³C] pyruvate using spectral-spatial excitation. *Magn Reson Med* 2013; 69:1209–1216.
32. Leupold J, Månsson S, Petersson JS, Hennig J, Wieben O. Fast multiecho balanced SSFP metabolite mapping of (¹H) and hyperpolarized (¹³C) compounds. *MAGMA* 2009; 22:251–256.
33. Hansen ES, Stewart NJ, Wild JM, Stødkilde-Jørgensen H, Laustsen C. Hyperpolarized ¹³C, ¹⁵N₂-urea MRI for assessment of the urea gradient in the porcine kidney. *Magn Reson Med* 2016; 76:1895–1899.
34. Abragam A, Goldman M. Principles of dynamic nuclear polarisation. *Rep Prog Phys* 1978; 41:395–467.
35. Lumata L, Merritt ME, Malloy CR, Sherry AD, Kovacs Z. Impact of Gd³⁺ on DNP of [1-¹³C]pyruvate doped with trityl OX063, BDPA, or 4-oxo-TEMPO. *J Phys Chem A* 2012; 116:5129–5138.
36. Ardenkjaer-Larsen JH, Macholl S, Jóhannesson H. Dynamic nuclear polarization with Trityls at 1.2 K. *Appl Magn Reson* 2008; 34:509–522.
37. Wenckebach T. Essentials of dynamic nuclear polarization. The Netherlands: Spindrift Publications, 2016; 296.
38. Overhauser AW. Polarization of nuclei in metals. *Phys Rev* 1953; 92:411–415.
39. Comment A, van den Brandt B, Uffmann K, et al. Design and performance of a DNP prepolarizer coupled to a rodent MRI scanner. *Concepts Magn Reson Part B Magn Reson Eng* 2007; 31B:255–269.
40. Ardenkjaer-Larsen JH, Bowen S, Petersen JR, et al. Cryogen-free dissolution dynamic nuclear polarization polarizer operating at 3.35 T, 6.70 T, and 10.1 T. *Magn Reson Med* 2019; 81:2184–2194.
41. Hövener JB, Pravdivtsev AN, Kidd B, et al. Parahydrogen-based hyperpolarization for biomedicine. *Angew Chem Int Ed Engl* 2018; 57:11140–11162.
42. Buljubasich L, Franzoni MB, Münnemann K. Parahydrogen Induced polarization by homogeneous catalysis: theory and applications. *Top Curr Chem* 2013; 328:33–74.
43. Pravica MG, Weitekamp DP. Net NMR alignment by adiabatic transport of parahydrogen addition products

- to high magnetic field. *Chem Phys Lett* 1988; 145: 255–258.
44. Dechent JF, Buljubasich L, Schreiber LM, Spiess HW, Münnemann K. Proton magnetic resonance imaging with para-hydrogen induced polarization. *Phys Chem Chem Phys* 2012; 14:2346–2352.
 45. Kovtunov KV, Barskiy DA, Coffey AM, et al. High-resolution 3D proton MRI of hyperpolarized gas enabled by parahydrogen and Rh/TiO₂ heterogeneous catalyst. *Chemistry* 2014; 20:11636–11639.
 46. Haake M, Natterer J, Bargon J. Efficient NMR pulse sequences to transfer the parahydrogen-induced polarization to hetero nuclei. *J Am Chem Soc* 1996; 118:8688–8691.
 47. Goldman M, Jóhannesson H. Conversion of a proton pair para order into ¹³C polarization by rf irradiation, for use in MRI. *Comp Rend Phys* 2005; 6:575–581.
 48. Kadlecsek S, Emami K, Ishii M, Rizi R. Optimal transfer of spin-order between a singlet nuclear pair and a heteronucleus. *J Magn Reson* 2010; 205:9–13.
 49. Golman K, Axelsson O, Jóhannesson H, Månsson S, Olofsson C, Petersson JS. Parahydrogen-induced polarization in imaging: subsecond (¹³C) angiography. *Magn Reson Med* 2001; 46:1–5.
 50. Jóhannesson H, Axelsson O, Karlsson M. Transfer of parahydrogen spin order into polarization by diabatic field cycling. *Comp Rend Phys* 2004; 5:315–324.
 51. Cavallari E, Carrera C, Boi T, Aime S, Reineri F. Effects of magnetic field cycle on the polarization transfer from parahydrogen to heteronuclei through long-range J-couplings. *J Phys Chem B* 2015; 119:10035–10041.
 52. Bär S, Lange T, Leibfritz D, Hennig J, von Elverfeldt D, Hövener JB. On the spin order transfer from parahydrogen to another nucleus. *J Magn Reson* 2012; 225:25–35.
 53. Stewart NJ, Kumeta H, Tomohiro M, Hashimoto T, Hatae N, Matsumoto S. Long-range heteronuclear J-coupling constants in esters: implications for (¹³C) metabolic MRI by side-arm parahydrogen-induced polarization. *J Magn Reson* 2018; 296:85–92.
 54. Gamliel A, Allouche-Arnon H, Nalbandian R, Barzilay CM, Gomori JM, Katz-Brull R. An apparatus for production of isotopically and spin-enriched hydrogen for induced polarization studies. *Appl Magn Reson* 2010; 39:329–345.
 55. Hövener JB, Bär S, Leupold J, et al. A continuous-flow, high-throughput, high-pressure parahydrogen converter for hyperpolarization in a clinical setting. *NMR Biomed* 2013; 26:124–131.
 56. Wagner S. Conversion rate of para-hydrogen to ortho-hydrogen by oxygen: implications for PHIP gas storage and utilization. *MAGMA* 2014; 27:195–199.
 57. Kadlecsek S, Vahdat V, Nakayama T, Ng D, Emami K, Rizi R. A simple and low-cost device for generating hyperpolarized contrast agents using parahydrogen. *NMR Biomed* 2011; 24:933–942.
 58. Hövener JB, Chekmenev EY, Harris KC, et al. PASADENA hyperpolarization of ¹³C biomolecules: equipment design and installation. *MAGMA* 2009; 22:111–121.
 59. Coffey AM, Shchepin RV, Truong ML, Wilkens K, Pham W, Chekmenev EY. Open-source automated parahydrogen hyperpolarizer for molecular imaging using ¹³C metabolic contrast agents. *Anal Chem* 2016; 88:8279–8288.
 60. Chukanov NV, Salnikov OG, Shchepin RV, Kovtunov KV, Koptuyug IV, Chekmenev EY. Synthesis of unsaturated precursors for parahydrogen-induced polarization and molecular imaging of 1-¹³C-acetates and 1-¹³C-pyruvates via side arm hydrogenation. *ACS Omega* 2018; 3:6673–6682.
 61. Schmidt AB, Berner S, Schimpf W, et al. Liquid-state carbon-13 hyperpolarization generated in an MRI system for fast imaging. *Nat Commun* 2017; 8:14535.
 62. Dang CV. Links between metabolism and cancer. *Genes Dev* 2012; 26:877–890.
 63. Zhu A, Lee D, Shim H. Metabolic positron emission tomography imaging in cancer detection and therapy response. *Semin Oncol* 2011; 38:55–69.
 64. Fletcher JW, Djulbegovic B, Soares HP, et al. Recommendations on the use of ¹⁸F-FDG PET in oncology. *J Nucl Med* 2008; 49:480–508.
 65. Golman K, Ardenkjaer-Larsen JH, Petersson JS, Mansson S, Leunbach I. Molecular imaging with endogenous substances. *Proc Natl Acad Sci U S A* 2003; 100:10435–10439.
 66. Marjańska M, Iltis I, Shestov AA, et al. *In vivo* ¹³C spectroscopy in the rat brain using hyperpolarized [1-(¹³C)]pyruvate and [2-(¹³C)]pyruvate. *J Magn Reson* 2010; 206:210–218.
 67. Golman K, in 't Zandt R, Thaning M. Real-time metabolic imaging. *Proc Natl Acad Sci U S A* 2006; 103: 11270–11275.
 68. Golman K, Zandt RI, Lerche M, Pehrson R, Ardenkjaer-Larsen JH. Metabolic imaging by hyperpolarized ¹³C magnetic resonance imaging for *in vivo* tumor diagnosis. *Cancer Res* 2006; 66:10855–10860.
 69. Warburg O. On the origin of cancer cells. *Science* 1956; 123:309–314.
 70. Albers MJ, Bok R, Chen AP, et al. Hyperpolarized ¹³C lactate, pyruvate, and alanine: noninvasive biomarkers for prostate cancer detection and grading. *Cancer Res* 2008; 68:8607–8615.
 71. Xu HN, Kadlecsek S, Profka H, Glickson JD, Rizi R, Li LZ. Is higher lactate an indicator of tumor metastatic risk? A pilot MRS study using hyperpolarized (¹³C)-pyruvate. *Acad Radiol* 2014; 21:223–231.
 72. Keshari KR, Sriram R, Koelsch BL, et al. Hyperpolarized ¹³C-pyruvate magnetic resonance reveals rapid lactate export in metastatic renal cell carcinomas. *Cancer Res* 2013; 73:529–538.
 73. Hu S, Balakrishnan A, Bok RA, et al. ¹³C-pyruvate imaging reveals alterations in glycolysis that precede c-Myc-induced tumor formation and regression. *Cell Metab* 2011; 14: 131–142.
 74. Day SE, Kettunen MI, Gallagher FA, et al. Detecting tumor response to treatment using hyperpolarized ¹³C magnetic resonance imaging and spectroscopy. *Nat Med* 2007; 13:1382–1387.
 75. Chen AP, Chu W, Gu YP, Cunningham CH. Probing early tumor response to radiation therapy using hyperpolarized [1-¹³C]pyruvate in MDA-MB-231 Xenografts. *PLoS One* 2013; 8:e56551.
 76. Saito K, Matsumoto S, Takakusagi Y, et al. ¹³C-MR spectroscopic imaging with hyperpolarized [1-¹³C]pyruvate detects early response to radiotherapy in SCC tumors and HT-29 tumors. *Clin Cancer Res* 2015; 21:5073–5081.

77. Park I, Bok R, Ozawa T, et al. Detection of early response to temozolomide treatment in brain tumors using hyperpolarized ¹³C MR metabolic imaging. *J Magn Reson Imaging* 2011; 33:1284–1290.
78. Dutta P, Le A, Vander Jagt DL, et al. Evaluation of LDH-A and glutaminase inhibition *in vivo* by hyperpolarized ¹³C-pyruvate magnetic resonance spectroscopy of tumors. *Cancer Res* 2013; 73:4190–4195.
79. Witney TH, Kettunen MI, Day SE, et al. A comparison between radiolabeled fluorodeoxyglucose uptake and hyperpolarized ¹³C-labeled pyruvate utilization as methods for detecting tumor response to treatment. *Neoplasia* 2009; 11:574–582.
80. Cunningham CH, Lau JYC, Chen AP, et al. Hyperpolarized ¹³C metabolic MRI of the human heart. *Circ Res* 2016; 119:1177–1182.
81. Grist JT, McLean MA, Riemer F, et al. Quantifying normal human brain metabolism using hyperpolarized [1-¹³C] pyruvate and magnetic resonance imaging. *Neuroimage* 2019; 189:171–179.
82. Aggarwal R, Vigneron DB, Kurhanewicz J. Hyperpolarized 1-[¹³C]-pyruvate Magnetic resonance imaging detects an early metabolic response to androgen ablation therapy in prostate cancer. *Eur Urol* 2017; 72:1028–1029.
83. Zhu Z, Marco-Rius I, Ohliger MA, et al. Hyperpolarized ¹³C dynamic breath-held molecular imaging to detect targeted therapy response in patients with liver metastases. In: *International Society for Magnetic Resonance in Medicine, Hawaii*. 2017; p. 1115.
84. Park I, Larson PEZ, Gordon JW, et al. Development of methods and feasibility of using hyperpolarized carbon-13 imaging data for evaluating brain metabolism in patient studies. *Magn Reson Med* 2018; 80:864–873.
85. Miloushev VZ, Granlund KL, Boltyanskiy R, et al. Metabolic imaging of the human brain with hyperpolarized ¹³C pyruvate demonstrates ¹³C Lactate production in brain tumor patients. *Cancer Res* 2018; 78:3755–3760.
86. Woitek R, McLean MA, Grist JT, et al. Imaging metabolic heterogeneity in breast cancer using hyperpolarized ¹³C-MRSI. In: *International Society for Magnetic Resonance in Medicine, Montreal*. 2019; p. 0258.
87. Villanueva-Mayer J, Autry A, Gordon J, et al. Serial HP [1-¹³C] pyruvate and 1H metabolic imaging in multiply recurrent high-grade glioma. In: *International Society for Magnetic Resonance in Medicine, Montreal*. 2019; p. 2868.
88. Autry AW, Gordon JW, Chen HY, et al. Serial characterization of HP [1-¹³C]pyruvate metabolism in the brains of patients with glioma and healthy controls. In: *International Society for Magnetic Resonance in Medicine, Montreal*. 2019; p. 0860.
89. Gutte H, Hansen AE, Larsen MM, et al. Simultaneous hyperpolarized ¹³C-pyruvate MRI and ¹⁸F-FDG PET (HyperPET) in 10 dogs with cancer. *J Nucl Med* 2015; 56:1786–1792.
90. Gutte H, Hansen AE, Henriksen ST, et al. Simultaneous hyperpolarized (13)C-pyruvate MRI and (18)F-FDG-PET in cancer (hyperPET): feasibility of a new imaging concept using a clinical PET/MRI scanner. *Am J Nucl Med Mol Imaging* 2015; 5:38–45.
91. Daniels CJ, McLean MA, Schulte RF, et al. A comparison of quantitative methods for clinical imaging with hyperpolarized (¹³C)-pyruvate. *NMR Biomed* 2016; 29:387–399.
92. Harrison C, Yang C, Jindal A, et al. Comparison of kinetic models for analysis of pyruvate-to-lactate exchange by hyperpolarized ¹³C NMR. *NMR Biomed* 2012; 25: 1286–1294.
93. Harris T, Eliyahu G, Frydman L, Degani H. Kinetics of hyperpolarized ¹³C1-pyruvate transport and metabolism in living human breast cancer cells. *Proc Natl Acad Sci U S A* 2009; 106:18131–18136.
94. Keshari KR, Wilson DM. Chemistry and biochemistry of ¹³C hyperpolarized magnetic resonance using dynamic nuclear polarization. *Chem Soc Rev* 2014; 43:1627–1659.
95. Schroeder MA, Lau AZ, Chen AP, et al. Hyperpolarized ¹³C magnetic resonance reveals early- and late-onset changes to *in vivo* pyruvate metabolism in the failing heart. *Eur J Heart Fail* 2013; 15:130–140.
96. Hu S, Yoshihara HAI, Bok R, et al. Use of hyperpolarized [1-¹³C]pyruvate and [2-¹³C]pyruvate to probe the effects of the anticancer agent dichloroacetate on mitochondrial metabolism *in vivo* in the normal rat. *Magn Reson Imaging* 2012; 30:1367–1372.
97. Chung BT, Chen HY, Gordon J, et al. First hyperpolarized [2-¹³C]pyruvate MR studies of human brain metabolism. *J Magn Reson* 2019; 309:106617.
98. Johansson E, Månsson S, Wirestam R, et al. Cerebral perfusion assessment by bolus tracking using hyperpolarized ¹³C. *Magn Reson Med* 2004; 51:464–472.
99. von Morze C, Larson PEZ, Hu S, et al. Imaging of blood flow using hyperpolarized [¹³C]urea in preclinical cancer models. *J Magn Reson Imaging* 2011; 33:692–697.
100. Lau AZ, Miller JJ, Robson MD, Tyler DJ. Simultaneous assessment of cardiac metabolism and perfusion using copolarized [1-¹³C]pyruvate and ¹³C-urea. *Magn Reson Med* 2017; 77:151–158.
101. Reed GD, von Morze C, Bok R, et al. High resolution ¹³C MRI with hyperpolarized urea: *in vivo* T₂ mapping and ¹⁵N labeling effects. *IEEE Trans Med Imaging* 2014; 33:362–371.
102. Laustsen C, Stokholm Nørlinger T, Christoffer Hansen D, et al. Hyperpolarized ¹³C urea relaxation mechanism reveals renal changes in diabetic nephropathy. *Magn Reson Med*. 2016; 75:515–518.
103. Gallagher FA, Kettunen MI, Hu DE, et al. Production of hyperpolarized [1,4-¹³C₂]malate from [1,4-¹³C₂] fumarate is a marker of cell necrosis and treatment response in tumors. *Proc Natl Acad Sci U S A* 2009; 106: 19801–19806.
104. Miller JJ, Lau AZ, Nielsen PM, et al. Hyperpolarized [1,4-¹³C₂]fumarate enables magnetic resonance-based imaging of myocardial necrosis. *JACC Cardiovasc Imaging* 2018; 11:1594–1606.
105. Clatworthy MR, Kettunen MI, Hu DE, et al. Magnetic resonance imaging with hyperpolarized [1,4-(13)C₂]fumarate allows detection of early renal acute tubular necrosis. *Proc Natl Acad Sci U S A* 2012; 109:13374–13379.
106. Witney TH, Kettunen MI, Hu DE, et al. Detecting treatment response in a model of human breast adenocarcinoma using hyperpolarised [1-¹³C]pyruvate and [1,4-¹³C₂] fumarate. *Br J Cancer* 2010; 103:1400–1406.
107. Eldirdiri A, Clemmensen A, Bowen S, Kjær A, Ardenkjær-Larsen JH. Simultaneous imaging of hyperpolarized [1,4-¹³C₂]fumarate, [1-¹³C]pyruvate and ¹⁸F-FDG in a rat

- model of necrosis in a clinical PET/MR scanner. *NMR Biomed* 2017; 30. doi: 10.1002/nbm.3803.
108. Bohndiek SE, Kettunen MI, Hu DE, et al. Hyperpolarized [1-¹³C]-ascorbic and dehydroascorbic acid: vitamin C as a probe for imaging redox status *in vivo*. *J Am Chem Soc* 2011; 133:11795–11801.
 109. Keshari KR, Kurhanewicz J, Bok R, Larson PEZ, Vigneron DB, Wilson DM. Hyperpolarized ¹³C dehydroascorbate as an endogenous redox sensor for *in vivo* metabolic imaging. *Proc Natl Acad Sci U S A* 2011; 108:18606–18611.
 110. Keshari KR, Wilson DM, Sai V, et al. Noninvasive *in vivo* imaging of diabetes-induced renal oxidative stress and response to therapy using hyperpolarized ¹³C dehydroascorbate magnetic resonance. *Diabetes* 2015; 64:344–352.
 111. Baligand C, Qin H, True-Yasaki A, et al. Hyperpolarized ¹³C magnetic resonance evaluation of renal ischemia reperfusion injury in a murine model. *NMR Biomed* 2017; 30. doi: 10.1002/nbm.3765.
 112. Gallagher FA, Kettunen MI, Brindle KM. Imaging pH with hyperpolarized ¹³C. *NMR Biomed* 2011; 24:1006–1015.
 113. Gallagher FA, Kettunen MI, Day SE, et al. Magnetic resonance imaging of pH *in vivo* using hyperpolarized ¹³C-labelled bicarbonate. *Nature* 2008; 453:940–943.
 114. Schroeder MA, Swietach P, Atherton HJ, et al. Measuring intracellular pH in the heart using hyperpolarized carbon dioxide and bicarbonate: a ¹³C and ³¹P magnetic resonance spectroscopy study. *Cardiovasc Res* 2010; 86: 82–91.
 115. Lau AZ, Miller JJ, Tyler DJ. Mapping of intracellular pH in the *in vivo* rodent heart using hyperpolarized [1-¹³C] pyruvate. *Magn Reson Med* 2017; 77:1810–1817.
 116. Düwel S, Hundshammer C, Gersch M, et al. Imaging of pH *in vivo* using hyperpolarized ¹³C-labelled zymonic acid. *Nat Commun* 2017; 8:15126.
 117. Chaumeil MM, Larson PEZ, Woods SM, et al. Hyperpolarized [1-¹³C] glutamate: a metabolic imaging biomarker of IDH1 mutational status in glioma. *Cancer Res* 2014; 74:4247–4257.
 118. Harris T, Degani H, Frydman L. Hyperpolarized ¹³C NMR studies of glucose metabolism in living breast cancer cell cultures. *NMR Biomed* 2013; 26:1831–1843.
 119. Rodrigues TB, Serrao EM, Kennedy BW, Hu DE, Kettunen MI, Brindle KM. Magnetic resonance imaging of tumor glycolysis using hyperpolarized ¹³C-labeled glucose. *Nat Med* 2014; 20:93–97.
 120. Koellisch U, Gringeri CV, Rancan G, et al. Metabolic imaging of hyperpolarized [1-¹³C]acetate and [1-¹³C]acetylcarnitine - investigation of the influence of dobutamine induced stress. *Magn Reson Med* 2015; 74:1011–1018.
 121. Flori A, Liserani M, Frijia F, et al. Real-time cardiac metabolism assessed with hyperpolarized [1-¹³C]acetate in a large-animal model. *Contrast Media Mol Imaging* 2015; 10:194–202.
 122. Bastiaansen JAM, Cheng T, Mishkovsky M, Duarte JMN, Comment A, Gruetter R. *In vivo* enzymatic activity of acetylCoA synthetase in skeletal muscle revealed by ¹³C turnover from hyperpolarized [1-¹³C]acetate to [1-¹³C]acetylcarnitine. *Biochim Biophys Acta* 2013; 1830: 4171–4178.
 123. Reineri F, Viale A, Dastrù W, Gobetto R, Aime S. How to design ¹³C para-hydrogen-induced polarization experiments for MRI applications. *Contrast Media Mol Imaging* 2011; 6:77–84.
 124. Bhattacharya P, Chekmenev EY, Perman WH, et al. Towards hyperpolarized ¹³C-succinate imaging of brain cancer. *J Magn Reson* 2007; 186:150–155.
 125. Chekmenev EY, Hövener J, Norton VA, et al. PASADENA hyperpolarization of succinic acid for MRI and NMR spectroscopy. *J Am Chem Soc* 2008; 130:4212–4213.
 126. Zacharias NM, McCullough CR, Wagner S, et al. Towards real-time metabolic profiling of cancer with hyperpolarized succinate. *J Mol Imaging Dyn* 2016; 6. pii: 123.
 127. Zacharias NM, Chan HR, Sailasuta N, Ross BD, Bhattacharya P. Real-time molecular imaging of tricarboxylic acid cycle metabolism *in vivo* by hyperpolarized 1-¹³C diethyl succinate. *J Am Chem Soc* 2012; 134:934–943.
 128. Goldman M, Jóhannesson H, Axelsson O, Karlsson M. Hyperpolarization of ¹³C through order transfer from parahydrogen: a new contrast agent for MRI. *Magn Reson Imaging* 2005; 23:153–157.
 129. Bhattacharya P, Harris K, Lin AP, et al. Ultra-fast three dimensional imaging of hyperpolarized ¹³C *in vivo*. *MAGMA* 2005; 18:245–256.
 130. Schmidt AB, Berner S, Braig M, et al. *In vivo* ¹³C-MRI using SAMBADENA. *PLoS One* 2018; 13:e0200141.
 131. Goldman M, Jóhannesson H, Axelsson O, Karlsson M. Design and implementation of ¹³C hyper polarization from para-hydrogen, for new MRI contrast agents. *Comp Rend Chim* 2006; 9:357–363.
 132. Cai C, Coffey AM, Shchepin RV, Chekmenev EY, Waddell KW. Efficient transformation of parahydrogen spin order into heteronuclear magnetization. *J Phys Chem B* 2013; 117:1219–1224.
 133. Bhattacharya P, Chekmenev EY, Reynolds WF, et al. Parahydrogen-induced polarization (PHIP) hyperpolarized MR receptor imaging *in vivo*: a pilot study of ¹³C imaging of atheroma in mice. *NMR Biomed* 2011; 24:1023–1028.
 134. Hurd RE, Yen YF, Mayer D, et al. Metabolic imaging in the anesthetized rat brain using hyperpolarized [1-¹³C] pyruvate and [1-¹³C] ethyl pyruvate. *Magn Reson Med* 2010; 63:1137–1143.
 135. Shchepin RV, Coffey AM, Waddell KW, Chekmenev EY. PASADENA hyperpolarized ¹³C phospholactate. *J Am Chem Soc* 2012; 134:3957–3960.
 136. Shchepin RV, Pham W, Chekmenev EY. Dephosphorylation and biodistribution of 1-¹³C-phospholactate *in vivo*. *J Labelled Comp Radiopharm* 2014; 57:517–524.
 137. Shchepin RV, Coffey AM, Waddell KW, Chekmenev EY. Parahydrogen induced polarization of 1-¹³C-phospholactate-*d*₂ for biomedical imaging with >30,000,000-fold NMR signal enhancement in water. *Anal Chem* 2014; 86:5601–5605.
 138. Reineri F, Santelia D, Viale A, et al. Para-hydrogenated glucose derivatives as potential ¹³C-hyperpolarized probes for magnetic resonance imaging. *J Am Chem Soc* 2010; 132:7186–7193.
 139. Reineri F, Viale A, Ellena S, et al. ¹⁵N Magnetic resonance hyperpolarization via the reaction of parahydrogen

- with ¹⁵N-propargylcholine. *J Am Chem Soc* 2012; 134: 11146–11152.
140. Shchepin RV, Chekmenev EY. Synthetic approach for unsaturated precursors for parahydrogen induced polarization of choline and its analogs. *J Label Compd Radiopharm* 2013; 56:655–662.
 141. McCormick J, Korchak S, Mamone S, et al. More than 12% polarization and 20 minute lifetime of ¹⁵N in a choline derivative utilizing parahydrogen and a rhodium nanocatalyst in water. *Angew Chem Int Ed Engl* 2018; 57:10692–10696.
 142. Reineri F, Boi T, Aime S. ParaHydrogen induced polarization of ¹³C carboxylate resonance in acetate and pyruvate. *Nat Commun* 2015; 6:5858.
 143. Cavallari E, Carrera C, Aime S, Reineri F. ¹³C MR hyperpolarization of lactate by using parahydrogen and metabolic transformation *in vitro*. *Chemistry* 2017; 23: 1200–1204.
 144. Cavallari E, Carrera C, Aime S, Reineri F. Studies to enhance the hyperpolarization level in PHIP-SAH-produced C13-pyruvate. *J Magn Reson* 2018; 289:12–17.
 145. Cavallari E, Carrera C, Sorge M, et al. The ¹³C hyperpolarized pyruvate generated by ParaHydrogen detects the response of the heart to altered metabolism in real time. *Sci Rep* 2018; 8:8366.
 146. Salnikov OG, Chukanov NV, Shchepin RV, et al. Parahydrogen-induced polarization of 1-¹³C-acetates and 1-¹³C-pyruvates using sidearm hydrogenation of vinyl, allyl, and propargyl esters. *J Phys Chem C Nanomater Interfaces* 2019; 123:12827–12840.
 147. Korchak S, Mamone S, Glöggl S. Over 50% ¹H and ⁴C polarization for generating hyperpolarized metabolites—a para-hydrogen approach. *ChemistryOpen* 2018; 7: 672–676.
 148. Wilson DM, Keshari KR, Larson PE, et al. Multi-compound polarization by DNP allows simultaneous assessment of multiple enzymatic activities *in vivo*. *J Magn Reson* 2010; 205:141–147.
 149. Cho A, Eskandari R, Granlund KL, Keshari KR. Hyperpolarized [6-¹³C, ¹⁵N3]-arginine as a probe for *in vivo* arginase activity. *ACS Chem Biol* 2019; 14:665–673.
 150. Moreno KX, Harrison CE, Merritt ME, Kovacs Z, Malloy CR, Sherry AD. Hyperpolarized δ[1-¹³C]gluconolactone as a probe of the pentose phosphate pathway. *NMR Biomed* 2017; 30:e3713.
 151. Park JM, Wu M, Datta K, et al. Hyperpolarized sodium [1-¹³C]-glycerate as a probe for assessing glycolysis *in vivo*. *J Am Chem Soc* 2017; 139:6629–6634.
 152. Ardenkjaer-Larsen JH. On the present and future of dissolution-DNP. *J Magn Reson* 2016; 264:3–12.
 153. Glöggl S, Grunfeld AM, Ertas YN, et al. A nanoparticle catalyst for heterogeneous phase para-hydrogen-induced polarization in water. *Angew Chem Int Ed Engl* 2015; 54:2452–2456.
 154. Leutzsch M, Wolf LM, Gupta P, et al. Formation of ruthenium carbenes by *gem*-hydrogen transfer to internal alkynes: implications for alkyne *trans*-hydrogenation. *Angew Chem Int Ed Engl* 2015; 54:12431–12436.
 155. Ripka B, Eills J, Kouřilová H, Leutzsch M, Levitt MH, Münnemann K. Hyperpolarized fumarate *via* parahydrogen. *Chem Commun* 2018; 54:12246–12249.
 156. Barskiy DA, Ke LA, Li X, et al. Rapid catalyst capture enables metal-free *para*-hydrogen-based hyperpolarized contrast agents. *J Phys Chem Lett* 2018; 9:2721–2724.
 157. Bales LB, Kovtunov KV, Barskiy DA, et al. Aqueous, heterogeneous *para*-hydrogen-induced ¹⁵N polarization. *J Phys Chem C* 2017; 121:15304–15309.
 158. Nonaka H, Hirano M, Imakura Y, Takakusagi Y, Ichikawa K, Sando S. Design of a ¹⁵N molecular unit to achieve long retention of hyperpolarized spin state. *Sci Rep* 2017; 7:40104.
 159. Kuhn LT, Bommerich U, Bargon J. Transfer of parahydrogen-induced hyperpolarization to ¹⁹F. *J Phys Chem A* 2006; 110:3521–3526.
 160. Bouchard LS, Kovtunov KV, Burt SR, et al. Para-hydrogen-enhanced hyperpolarized gas-phase magnetic resonance imaging. *Angew Chem Int Ed Engl* 2007; 46: 4064–4068.
 161. Kovtunov KV, Truong ML, Barskiy DA, et al. Propane-*d*₆ heterogeneously hyperpolarized by parahydrogen. *J Phys Chem C* 2014; 118:28234–28243.
 162. Hövener JB, Schwaderlapp N, Borowiak R, et al. Toward biocompatible nuclear hyperpolarization using signal amplification by reversible exchange: quantitative *in situ* spectroscopy and high-field imaging. *Anal Chem* 2014; 86:1767–1774.
 163. Hurd RE, Yen YF, Chen A, Ardenkjaer-Larsen JH. Hyperpolarized ¹³C metabolic imaging using dissolution dynamic nuclear polarization. *J Magn Reson Imaging* 2012; 36:1314–1328.
 164. Kohler SJ, Yen Y, Wolber J, et al. *In vivo* 13 carbon metabolic imaging at 3T with hyperpolarized ¹³C-1-pyruvate. *Magn Reson Med* 2007; 58:65–69.
 165. Josan S, Hurd R, Park JM, et al. Dynamic metabolic imaging of hyperpolarized [2-¹³C]pyruvate using spiral chemical shift imaging with alternating spectral band excitation. *Magn Reson Med* 2014; 71:2051–2058.
 166. Salamanca-Cardona L, Keshari KR. ¹³C-labeled biochemical probes for the study of cancer metabolism with dynamic nuclear polarization-enhanced magnetic resonance imaging. *Cancer Metab* 2015; 3:9.
 167. Park JM, Josan S, Grafendorfer T, et al. Measuring mitochondrial metabolism in rat brain *in vivo* using MR spectroscopy of hyperpolarized [2-¹³C]pyruvate. *NMR Biomed* 2013; 26:1197–1203.